Abstract Recent progress in chromium and iron doped II-VI semiconductor materials makes them the laser sources of choice when one needs a compact system with tunability over 1.9–5.1 µm. Output powers exceeding 10 W and efficiency up to 70% were demonstrated in several Cr doped semiconductors. The unique combination of technological (low-cost ceramic material) and spectroscopic characteristics makes these materials ideal candidates for mid-IR tunable laser systems. This article reviews transition metal doped II–VI materials and recent progress in Cr- and Fe-doped solid-state mid-IR lasers.

Critical areas driving future progress in Cr- and Fe-doped chalcogenide middle infrared lasers: fabrication of binary and ternary II–VI ceramic gain media with low phonon cut-off, low optical losses and high design flexibility; high performance laser design with improved characteristics in power (power scaling to dozens of Watts), spectral (spectral coverage over 1.8–6 µm), temporal (frequency comb generation), and pump domains (electrically pumped Cr- and Fe-doped II–VI quantum confined structures).

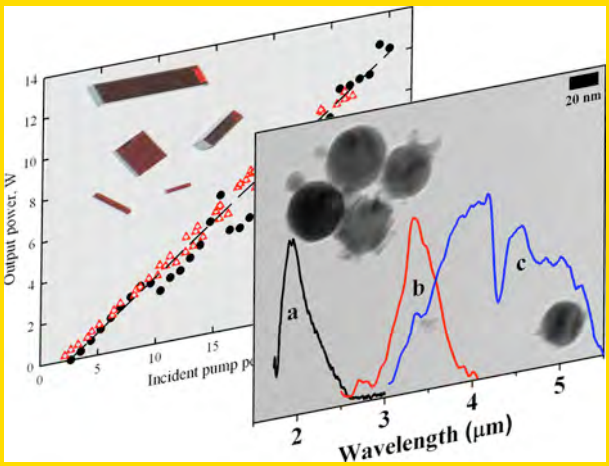

© 2010 by WILEY-VCH Verlag GmbH & Co. KGaA, Weinheim

Progress in Cr^{2+} and Fe^{2+} doped mid-IR laser materials

Sergey Mirov[1,2,*], *Vladimir Fedorov*[1,2], *Igor Moskalev*[1,2], *Dmitri Martyshkin*[1,2], *and Changsu Kim*[1]

[1] Center for Optical Sensors and Spectroscopies and the Department of Physics, University of Alabama at Birmingham, CH 310, 1300 University Blvd., Birmingham, AL 35294, USA
[2] Photonics Innovations, Inc., 1500 1st Avenue South, Suite L108, Birmingham, AL 35203, USA

Received: 27 November 2008, Revised: 4 February 2009, Accepted: 4 February 2009
Published online: 16 March 2009

Key words: Solid-state lasers, tunable lasers, mid-IR lasers, random lasers, laser ceramic, quantum dots lasers.

PACS: 42.55.Rz, 42.55.Zz, 71.55.Gs, 78.55.-m, 78.60.Fi, 78.67.-n

1. Introduction

Middle-infrared (mid-IR) laser sources operating over the "molecular fingerprint" 2–15 µm spectral range are in great demand for a variety of applications including molecular spectroscopy, non-invasive medical diagnostics, industrial process control, environmental monitoring, atmospheric sensing and free space communication, oil prospecting, and numerous defense related applications such as infrared countermeasures, monitoring of munitions disposal, and stand-off detection of explosion hazards. Mid-IR wavelengths are usually generated using relatively complex nonlinear optical conversion techniques or by means of direct generation in hetero-junction lead-salt, antimonide, or quantum cascade semiconductor lasers featuring limited output power and tuning range. Impurity doped crystalline lasers constitute another viable route for mid-IR coherent sources. Comprehensive reviews of mid-IR lasers based on insulating crystals doped with rare-earth ions were published by Kaminski [1, 2]. Transition metal (TM^{2+}, e.g., Cr^{2+} or Fe^{2+}) doped binary (e.g., ZnSe, ZnS, CdSe, CdS, ZnTe) and ternary (e.g., CdMnTe, CdZnTe, ZnSSe) chalcogenide crystals, having a gain bandwidth up to 50% of central wavelength, represent another class of solid state gain media with strong and ultra-broad absorption and emission bands in the mid-IR range of optical spectra. In 1996 scien-

* Corresponding author: e-mail: mirov@uab.edu

© 2010 by WILEY-VCH Verlag GmbH & Co. KGaA, Weinheim

tists from the Lawrence Livermore National Laboratory [3] were the first to show that among different types of crystalline gain materials TM^{2+} doped wide bandgap II–VI semiconductor crystals could be very special for mid-IR lasing:

- An important feature of the II–VI compounds is their tendency to crystallize as tetrahedral coordinated structures, as opposed to the typical octahedral coordination at the dopant site. Tetrahedral coordination gives smaller crystal field splitting, placing the dopant transitions further into the IR.
- Another key feature of these materials is that the heavy anions in the crystals provide a very low energy optical phonon cutoff that makes them transparent in a wide spectral region and decreases the efficiency of non-radiative decay, which gives promise of a high yield of fluorescence at room temperature (RT).

Active interest in TM doped II–VI compounds inspired by [3] was explained by the fact that these media are close mid-IR analogs of the titanium-doped sapphire (Ti-S) in terms of spectroscopic and laser characteristics. It was anticipated that TM^{2+} doped chalcogenides would lase in the mid-IR with a great variety of possible modes of oscillation, similar to the Ti-S laser. Indeed, optically pumped RT lasers based on Cr:ZnS, Cr:ZnSe, Cr:$Cd_{1-x}Mn_xTe$, Cr:CdSe, and Fe:ZnSe crystals providing access to the 2–5 µm spectral region with high (up to 70%) efficiency, multi-Watt-level output powers, tunability in excess of 1000 nm, and narrow spectral linewidth (< 20 MHz), have been reported by several groups (see reviews [4, 5] and references therein). Arguably these lasers represent nowadays the simplest and the most cost-effective route for high power, broadly tunable lasing in this 2–5 µm wavelength range. Below we will present recent progress in developing chromium and iron doped lasers.

2. Spectroscopic properties of the Fe^{2+} and Cr^{2+} ions

The ground state of the free Cr^{2+} ($3d^4$) and Fe^{2+}($3d^6$) ions is ^{5}D state with total degeneracy equal to $g = (1+2L)(1+2S) = 25$. Energy gaps to the other terms of free ions (^{3}H, ^{3}G, ^{3}F(2), ^{3}D, ^{3}P(2), ^{1}I, ^{1}G(2), ^{1}F, ^{1}D(2), ^{1}S(2)) can be calculated using only two *Racah parameters*: B and C. Empirical values of the Racah parameters for Cr^{2+}(Fe^{2+}) are equal to $B = 830(1058)$ and $C = 3430(3901)\,\mathrm{cm}^{-1}$, correspondingly [6]. The energy splitting between ground ^{5}D term and next ^{3}H term levels can be calculated as follows: $\Delta E = E\left(^3\mathrm{H}\right) - E\left(^5\mathrm{D}\right) = 4C + 4B$ [6], which places transitions from the ^{5}D ground state to upper levels in the visible spectral range. The tetrahedral crystal field (T_d) of the II–VI semiconductors splits ^{5}D ground state into triplet $^5T_2$ and duplet ^{5}E. Energy splitting between these levels in the tetrahedral coordination corresponds to the mid-IR spectral range and can be estimated using crystal field theory as:

$$\Delta = \mathrm{E}\left(^5\mathrm{E}\right) - \mathrm{E}\left(^5\mathrm{T}_2\right) = 10Dq = \left(\frac{20}{27}\right)\frac{Q^2}{4\pi\varepsilon_0 a^5}\left\langle r^4\right\rangle_{3\mathrm{d}}, \quad (1)$$

where Dq is so-called *crystal field parameter*; Q is a ligand's charge; a is a distance between ligands and transition metals; $\left\langle r^4\right\rangle_{3\mathrm{d}}$ is the mean radius of the $3d$-electrons.

The $^5T_2$ and ^{5}E are the two lowest states for a system with $Dq/B < 1.2$. In the tetrahedral crystal field, doublet ^{5}E is the ground state of the iron ions, while $^5T_2$ is the ground state of the chromium ions. The transitions between these levels are spin-allowed. The rest of the transitions from ^{5}D levels are spin forbidden. For example, radiative lifetime of the Cr^{2+} ions at ^{5}E(^{5}D) $\leftrightarrow$ $^5T_2$(^{5}D) transition is around 6 µs, while the radiative lifetime at ^{3}H($^3T_2$) $\leftrightarrow$ ^{5}D ($^5T_2$, ^{5}E) transitions is around $\sim$ 1 ms. As a result, the excited-state absorption is negligible, making the ^{5}E $\leftrightarrow$ $^5T_2$ transition very promising for laser applications. Spin-orbit coupling and Jahn-Teller mechanism are responsible for further energy splitting of the terms. In addition, strong electron phonon coupling results in line broadening and a strong Stokes shift between absorption and emission bands.

The absorption and emission bands at ^{5}E $\leftrightarrow$ $^5T_2$ transition of some chromium-doped II–VI crystals are shown in Fig. 1. Among all the II–VI chalcogenides ZnS crystals feature the maximum ^{5}D term energy splitting due to the smallest inter-ligand distance (see Eq. 1 and Table 1). Therefore,

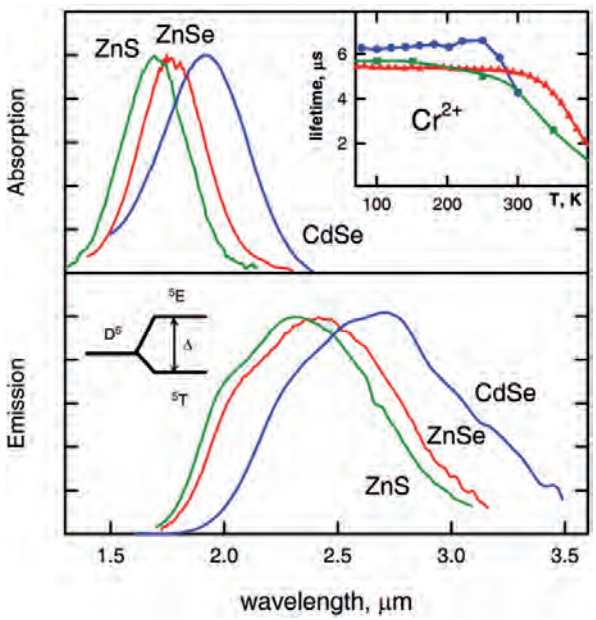

Figure 1 (online color at: www.lpr-journal.org) Normalized room temperature absorption and emission-gain spectra of Cr^{2+} ions in ZnS, ZnSe, and CdSe crystals. Insert shows temperature dependences of Cr^{2+} ions lifetimes in ZnS (circle), ZnSe (triangle), and CdSe (square) crystals.

© 2010 by WILEY-VCH Verlag GmbH & Co. KGaA, Weinheim

Table 1 Major material properties of ZnS, ZnSe, CdSe, and CdMnTe crystals.

Crystal	ZnS	ZnSe	CdSe	CdMnTe
Symmetry	C/H	C	H	C
Density, g/cm^3	4.08	5.26	5.81	
Bond length, nm	0.234	0.245	0.263	0.276
Band Gap, eV	3.9	2.8	1.7	2.1
Transparency range, μm	0.4–14	0.5–20	0.8–21	0.6–22
n @3.0 μm	2.26	2.44	2.5	2.5
$(1/n)(dn/dT)$, K^{-1}	1.9×10^{-5}	2.6×10^{-5}	4×10^{-5}	
Second order nonlinearity, pV/m	d_{eff}=8	d_{eff}=30	d_{31}=35	d_{14}=340
Third order of nonlinearity $\times 10^{20}$ m^2/W	84 @1.06 μm	460 @1.06 μm	1300 @1.5 μm	
Verdet constant, Deg/Tm	3024@0.63 μm	6700@0.63 μm	3300@0.98 μm	20000@0.98 μm
Specific Heat, J/gK	0.47	0.34	0.49	
Thermal conductivity, W/cm K	0.27	0.19	0.09	0.075
Hardness, Knoop	178	100	44–90	

(C – Cubic symmetry; H – Hexagonal symmetry; first neighbor distance calculated as $d = \left(\sqrt{3}/4\right) a$ for cubic crystals and $d = (3/8)\, c$ for hexagonal crystal [4, 7, 15, 16, 77].

the absorption and emission bands of chromium 5E $\leftrightarrow$ ^{5}T$_2$ transition in ZnS are shifted towards shorter wavelengths in comparison with the bands of other II–VI semiconductors. Conversely, Cr:CdSe crystals feature one of the biggest lattice parameter and have the longest-wavelength shifted bands. Broad absorption bands spanning over 1.5–2.2 μm spectral range with maxima at $\sim$ 1.7, 1.8, and 1.9 μm for ZnS, ZnSe, and CdSe, correspondingly, allow using a big variety of the pumping sources.

The laser oscillation of the Cr^{2+} ions in the II–VI semiconductor crystals has been already demonstrated using a direct optical excitation by the radiations of: $\sim$ 1.6 μm Er^{3+} bulk or fiber lasers; $\sim$ 1.9 μm Tm^{3+} bulk or fiber lasers; $\sim$ 2.1 μm Ho^{3+} bulk laser; $\sim$ 1.6 μm Raman Shifted Nd:YAG (1.064 μm); $\sim$ 1.6 μm NaCl:OH color center laser, $\sim$ 1.9 μm Co^{2+}:MgF_2 laser; 1.6–1.9 μm semiconductor InGaAsP/InP diode and semiconductor disk lasers. Some of these pump laser sources are commercially available with an output power in excess of several hundred watts in CW operation mode and with a more than one Joule of output energy in pulsed regime.

As shown in Fig. 1, Cr^{2+}:II–VI crystals feature broad emission bands with $(\Delta\lambda/\lambda) \sim 0.5$, which is very attractive for ultrashort pulse generation as well as for broad mid-IR tunability. The insert in Fig. 1 demonstrates temperature dependence of the luminescence lifetime at ^{5}E $\leftrightarrow$ ^{5}T$_2$ transition of chromium. There is no luminescence quenching in ZnSe crystal at RT which means that the luminescence quantum yield is close to unity in this crystal. It is one of the reasons why Cr:ZnSe crystal is currently most widely used when one needs a practical and efficient room temperature laser operating over 2–3 μm spectral range. RT fluorescence lifetime of Cr^{2+} in ZnS crystal drops by $\sim$ 25% in comparison with low temperature measurements. This difference can be explained by a higher phonon cutoff frequency of ZnS crystals ($\nu_{LO} \approx 330\,cm^{-1}$) in comparison with ZnSe ($\nu_{LO} \approx 250\,cm^{-1}$), as well as by higher probability of non-radioactive processes [7]. However, $\tau = 5\,\mu s$ luminescence lifetime is sufficient for effective RT lasing in Cr:ZnS crystal. A similar 25% drop of the Cr:CdSe RT quantum yield was reported in [8].

The peak absorption and emission cross-sections of Cr^{2+} calculated from the spectroscopic experiments [3–5] were of the order of $\sigma \sim 10^{-18}\,cm^2$ for all II–VI hosts. This value is about two orders of magnitude greater than emission cross-section values of the rare-earth ions. Therefore, Cr doped II–VI semiconductors, being effective gain materials for broadly tunable mid-IR lasers, are also very promising for passive Q-switching of the cavities of rare-earth (e.g., Er^{3+}, Tm^{3+}, Ho^{3+}) lasers.

The concentration quenching of luminescence of Cr:ZnSe crystals was studied in detail in [9,10]. The authors showed that concentration quenching could be neglected at RT at concentrations below $10^{19}\,cm^3$. However, the excited-state lifetime drastically decreases at higher concentrations.

Divalent iron ions have smaller effective radius than chromium ions. Therefore, their absorption and emission bands are shifted further to the mid-IR spectral range with respect to chromium ions (see Eq. 1). The RT absorption spectra of iron doped ZnSe and CdMnTe crystals are depicted in Fig. 2. The maximum absorption coefficient of Fe^{2+} ions is located at 3.1 and 3.6 μm in ZnSe and CdMnTe crystals, correspondingly. The bandwidths at full-width at half-maximum (FWHM) are equal to 1.37 (ZnSe) [11]

© 2010 by WILEY-VCH Verlag GmbH & Co. KGaA, Weinheim

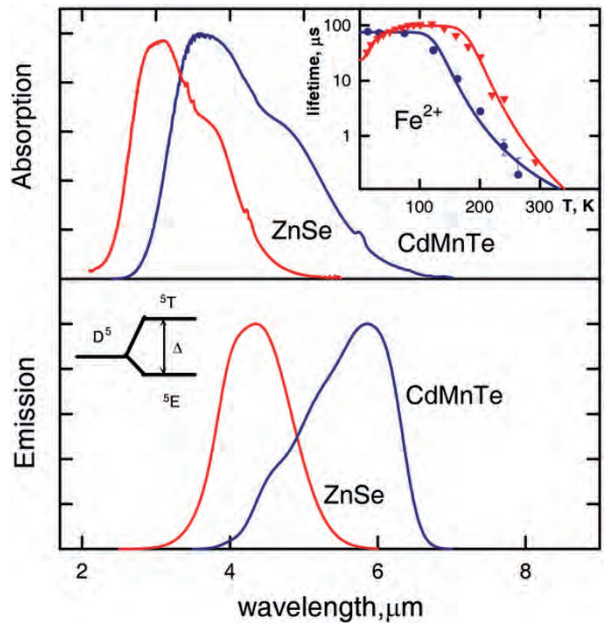

Figure 2 (online color at: www.lpr-journal.org) Normalized room temperature absorption and emission-gain spectra of Fe^{2+} ions in ZnSe and CdMnTe crystals. Insert shows temperature dependences of Cr^{2+} ions lifetimes in ZnSe (triangle) and CdMnTe (circle) crystals.

and 1.91 μm (CdMnTe) [12]. In spite of the fact that Fe^{2+} ions have a very broad absorption band, available pump sources are not as diverse as for Cr^{2+} ions. The iron lasing was demonstrated using pump 2.8–2.9 μm radiation of Er-lasers, radiation of Cr^{2+} lasers, and radiation of 2nd D_2 Raman Stokes of Nd:YAG (1.06 μm) with oscillation wavelengths ~ 2.92 μm. Additionally, laser-spectroscopic experiments [11] demonstrated several other excitation mechanisms of the Fe^{2+} ions over ionization processes under green excitation (532 nm) and over energy transfer from Cr^{2+} to Fe^{2+} in the co-doped crystals. These mechanisms could be also used for lasing excitation. The temperature dependences of the lifetime of Fe^{2+} ions in ZnSe and CdMnTe crystals are depicted in Fig. 2. The decreasing luminescence lifetime at temperatures higher than 120 K is due to thermally activated nonradiative decay. Nonradiative processes result in a luminescence lifetime as short as several hundreds of ns and low luminescence quantum yield at room temperature ($\eta \sim 1\%$). In papers [13, 14] a luminescence lifetime increase was reported for the 14–110 K temperature range. This can be explained either by thermal population of the sub-levels with smaller oscillator strength or by luminescence re-absorption effect due to strong overlapping of the absorption and emission bands. Table 2 summarizes spectroscopic characteristics of chromium and iron ions in ZnS, ZnSe, CdSe, and CdMnTe crystals. One can see that spectroscopic properties of Cr^{2+} and Fe^{2+} ions in the II–VI hosts enable tunable lasing over a broad mid-IR spectral range from 1.8 (Cr:ZnS) to 6.5 μm (Fe:CdMnTe).

Table 2 Spectroscopic characteristics of chromium and iron ions in ZnS, ZnSe, CdSe, and CdMnTe crystals. σ_{ab}, σ_{em} – peak absorption and emission cross-sections; λ_{ab}, λ_{em} – peak absorption and emission spectra wavelengths, respectively; τ_{rad} – radiative lifetime; τ_{RT} – excited-level lifetime at room temperature [3–5, 11, 12, 48, 76, 77].

	Cr^{2+}			Fe^{2+}	
	ZnS	**ZnSe**	**CdSe**	**ZnSe**	**CdMnTe**
Absorption					
$\sigma_{ab}, 10^{-20}$ cm^2	100	110	194	97	52
λ_{ab}, nm	1690	1770	1890	3100	3600
$\Delta\lambda_{ab}$, nm	350	350	440	1370	1910
Emission					
$\sigma_{em}, 10^{-20}$ cm^2	140	130	200	250	140
λ_{em}, nm	2350	2450	2650	4350	5760
$\Delta\lambda_{em}$, nm	820	860	940	1610	1400
τ_{rad}, μs	5.7	5.5	6.4	35	75
τ_{RT}, μs	4.3	5.4	4.4	0.37	0.1-0.2
$\eta = \tau_{RT}/\tau_{rad}$	0.8	~ 1	0.7	0.01	$\sim 10^{-3}$

3. Fabrication

Material properties

For decades, the pure and doped (Cu and Mn) wide-bandgap II–VI semiconductors have been called promising materials for the fabrication of light-emitting devices (LED) and phosphors for electro-luminescent displays and photovoltaic devices. Due to their high IR transparency these materials are widely used for IR optics as well. A variety of material fabrication techniques were developed for II–VI semiconductors. However, for most of the above applications, the chromium and iron ions were considered as undesirable impurities. The doping procedure with concentration and optical quality suitable for laser application were not developed until the first laser experiments demonstrated in the middle of 90's. The material properties of the most important Cr^{2+} and Fe^{2+} doped II–VI semiconductors are summarized in Table 1. Among all the II–VI semiconductors, ZnS and ZnSe crystals have the widest bandgaps and reveal the most favorable thermal-optical characteristics. The use of other materials is motivated by a smaller crystal field splitting of the TM ions, resulting in additional emission red shifting in comparison with ZnS and ZnSe hosts. For example, tunable laser oscillation with a wavelength longer than 3 μm is very important for spectroscopic and sensing applications, since many organic compounds have characteristic vibronic transitions in this spectral range. For this reason, Cr:CdSe laser systems tunable up to 3.6 μm are of special interest. It should be noted that in comparison with the best oxide crystal hosts, the II–VI semiconductors feature strong thermal lensing ($dn/dT = 49 \times 10^{-6}$ and 8.6×10^{-6} for ZnS and YAG correspondingly [15]). Therefore, proper thermal management is very important for power scaling of Cr and Fe doped chalcogenide lasers.

© 2010 by WILEY-VCH Verlag GmbH & Co. KGaA, Weinheim

Crystal growth

Different techniques were developed for fabrication of II–VI bulk materials (melt-growth technique; PVT, physical vapor transport; and CVT, chemical vapor transport) [16]. The melt growth technique (Bridgman) and PVT are the most commonly used techniques for single crystal fabrication. Under atmospheric pressure ZnSe sublimation occurs at a temperature above ~ 400 °C, which is lower than that of the melting point. One of the fundamental problems for the melt growth technique is sublimation of the crystal compounds. Therefore, to use melt growth techniques, it is necessary to simultaneously apply high pressure (75×10^2 KPa) and high temperature (1515 °C). For this reason, the Czochralski method has not been used widely for growth of II—VI compounds. High temperature melt growth is often accompanied by uncontrolled contamination. This contamination can lead to undesirable and parasitic absorptions. On the other hand, doping during PVT crystal growth is also very difficult in terms of achieving homogeneous impurity distribution with predicted concentration, especially in heavily doped single crystals. In spite of these difficulties, TM:II–VI single crystals with good laser characteristics were reported by several groups. More details on TM doped II–VI crystal fabrication are available in the following publications: Chromium doped- ZnSe (PVT [17, 18]), CdSe (PVT [19], gradient freezing [20]), $CdS_{1-x}Se_x$(PVT [19, 21]), CdTe (Bridgman [22]), $Cd_{1-x}Mn_xTe$ (Bridgman [22, 23]); Iron doped-ZnSe (PVT [17]), CdSe (Bridgman [24]), CdTe (Bridgman [24]), $Cd_{1-x}Mn_xTe$ (Bridgman [12]).

Thermal diffusion

The diffusion of the TM ions into II–VI semiconductors has been studied for more than 60 years (see, for example, [25]). This technique utilizes thermally activated diffusion of transition metal ions into II–VI crystals. Thermal diffusion is usually realized from the TM metal film deposited on the crystal surface or from the vapor phase. In the first case, Cr or Fe films are deposited on the crystal surface, using pulse-laser deposition, vapor deposition, or magnetron spattering system. At the second stage, thermal diffusion is carried out in sealed vacuumed ($\sim 10^{-5}$ torr) ampoules at temperature of 900–1100°C over 7–20 days. In the vapor phase diffusion method, II–VI samples together with TM (Cr, Fe, Co, Ni) or TM compounds (CrS, CrSe, FeSe) are placed in the different parts of the ampoules. The ampoules are sealed at low pressure and annealed. Thermal diffusion method in comparison with crystal growth is very cost-effective and simple. Thermal diffusion technique became widely used especially after it was demonstrated that laser characteristics of the TM doped II–VI single- and polycrystals are practically identical. As a result, the combination of the low-cost and readily available polycrystalline II–VI materials with effective and affordable post-growth TM doping procedure enables an effective technology for active elements fabrication, which is quite rare for solid-state laser materials. However, the thermal diffusion, by its nature, is usually accompanied by inhomogeneous distribution of the dopant over the diffusion length. In addition, an increase of the annealing time usually facilitates higher scattering losses. Therefore, preparation of large-scale samples with homogeneous TM ion distribution for power-scaling applications requires special technological contrivance. Recently, the thermal-diffusion technology for large-scale samples fabrication with homogeneous distribution of dopant concentration was developed (see Fig. 3). The specific details of the thermal-diffusion process are reported in [9, 26, 27].

Hot press ceramics

The idea that ceramic material will be optically indistinguishable from a single crystal of the same composition was proposed in 1960's. Later in 1966, hot-pressed CaF_2 doped with dysprosium was reported as the first successful ceramic laser material [28]. New interest in laser ceramic materials was stimulated by the progress in development of Nd:YAG ceramics by Konoshima Chemical Co. Ltd. [29]. Ceramic lasers in some cases surpass the output characteristics of lasers based on single crystal counterparts. Ceramic laser materials show promise not only for their laser and thermal-optical properties but also for their economics. The major advantage of laser ceramics is in advanced ceramic processing enabling affordable mass production and design flexibility of the laser elements (undoped ends, waveguiding structures, gradient of dopant concentration, etc) important for development of efficient, high performance lasers.

The first lasing of the Cr:ZnSe hot-pressed ceramic in the CW and gain switched regimes was demonstrated in [5, 30]. In these publications the authors fabricated Cr:ZnSe ceramic by a multi-step process involving powder preparation and a multi-step heating and pressing procedures. The powder preparation for hot-pressing was performed by mixing pure ZnSe and a preliminary prepared mixture of ZnSe-CrSe (1 mol %). This mixture contained particles with diameters less than 10 μm. Prior to hot pressing, the samples were first briquetted (cold-pressed) at room temperature under a pressure of 60 MPa. Samples with different CrSe concentrations were then further hot-pressed at 1400–1500 K at axial compression of up to 350 MPa. After 10–15 minutes of sintering, samples were cooled to room temperature. This fabrication technique is very promising for high power/energy mid-IR lasers based on transition metal doped chalcogenides.

Laser powders

Laser active TM:II–VI powders prepared without a stage of bulk crystal growth were recently reported in several publications [31, 32]. In these experiments Cr doped II–VI powders were prepared by annealing of the chemicals

© 2010 by WILEY-VCH Verlag GmbH & Co. KGaA, Weinheim

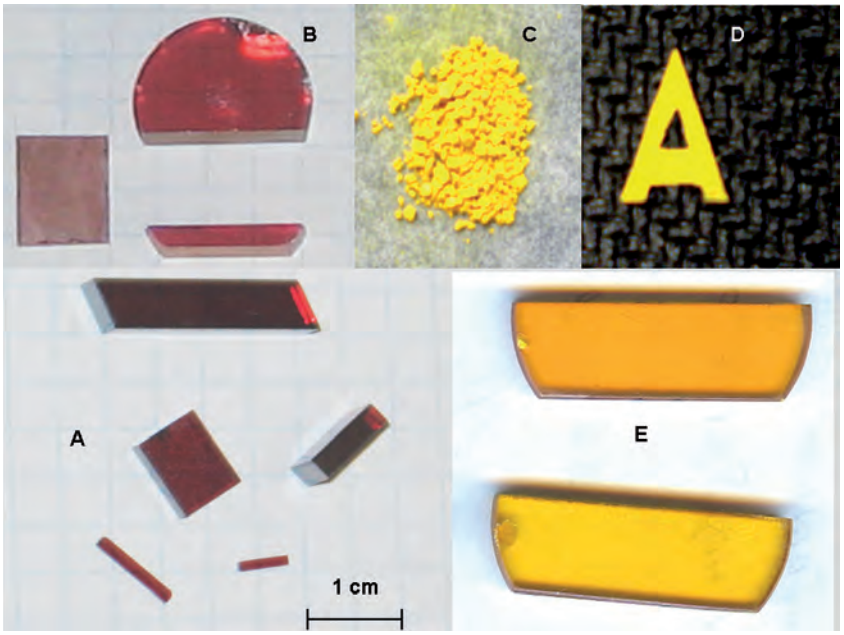

Figure 3 (online color at: www.lpr-journal.org) Chromium and Iron doped ZnSe laser gain media: A) Diffusion-doped Cr^{2+}:ZnSe crystals; B) Cr:ZnSe hot-press ceramics; C) Cr:ZnSe powder; D) Polymer Film (0.180 mm thick), cut in a form of a letter "A", based on a mixture of Cr^{2+}:ZnSe powder and Teflon (1:1 wt%); E) Fe:ZnSe poly- and single crystals.

(ZnSe:CrSe; ZnS:CrS; CdSe:CrSe) at 1000 °C for 6 days in sealed, evacuated ($\sim 10^{-4}$ Torr) quartz ampoules and were used for random lasing. In the random laser, the radiation feedback results not from cavity mirrors, as in conventional lasers, but from multiple random scattering in the gain medium [33]. High spectral brightness of the random lasers makes them interesting for optical coding applications. In addition to random lasing there were several other ideas inspiring the development of these laser active powders. One of them was to incorporate fabrication of these powders as a stand-alone step in hot-pressed ceramic technology for improving optical quality of the final product as well as for avoiding possible segregation of dopant near the grain boundaries. Development of composite thin film (e.g. TM:II–VI doped polymer) or mid-IR fiber (e.g. chalcogenides glass fiber impregnated with TM:II–VI) gain media was another motivation. Finally, it was believed that these media could be instrumental for development of future electro-luminescent devices as well as future electrically pumped mid-IR lasers.

TM doped II–VI thin-films

The wide-bandgap II–VI semiconductors have been regarded as promising materials for blue-green diode lasers. Therefore, most of II–VI thin film structures were developed for these applications. Spintronics is another important application area of the TM doped II–VI thin films. The diluted magnetic semiconductors (DMSs) have been intensively investigated for many years. Most of the early papers were devoted to materials doped by Cr, Mn, Fe, and Co ions. The mid-IR photoluminescence properties of the TM doped II–VI thin films were studied much less intensively. Cr doped II–VI semiconductor thin-film technology is crucial for developing the new type of mid-IR tunable solid-state lasers with electrical pumping. Realization of electrical excitation of Cr:II–VI media requires simultaneous solution of several fundamental physical problems including: efficient energy transfer from the charge carriers to TM impurities, donor-acceptor self-compensation, and possible chromium valence change in the co-doped materials.

A series of Cr-doped ZnSe and ZnTe epilayers for mid-IR optical studies were grown by molecular beam epitaxy (MBE) on semi-insulating GaAs (001) substrates [34–37]. Chromium concentrations in the doped epilayers ranged from 10^{14} to 10^{20} cm^{-3}. Incorporation of chromium in the active Cr^{2+} state in thin MBE grown epilayers was further verified by optical spectroscopy and direct comparison of the PL spectrum of thin film to that of bulk Cr:ZnSe grown for mid-IR laser applications.

Thin films of Cr:ZnSe grown by means of pulse laser deposition (PLD) were studied in [38]. Although the concentration of extended defects in PLD grown thin films is typically higher than those reported in MBE, the simplicity and versatility of PLD renders it ideal for low-cost, rapid prototyping of thin films in exploratory settings. Cr doped ZnSe thin films were grown by PLD on GaAs, sapphire, and Si substrates. The films on all three substrates were also polycrystalline with a typical thickness of 1–8 µm. The mid-IR photoluminescence was also reported for the Cr-doped ZnS nanocrystalline films synthesized by PLD on the Si (100) substrate [39].

Mid-IR photoluminescence associated with Fe^{2+} transitions in Fe-doped ZnSe thin layers was reported in [40]. 100 nm thick ZnSe epilayers were grown by MBE on GaAs semi-insulating substrates. The mid-IR emission spectrum at temperature $T = 20$ K shows the characteristic luminescence band around 3.7 µm. Besides possible applications

© 2010 by WILEY-VCH Verlag GmbH & Co. KGaA, Weinheim

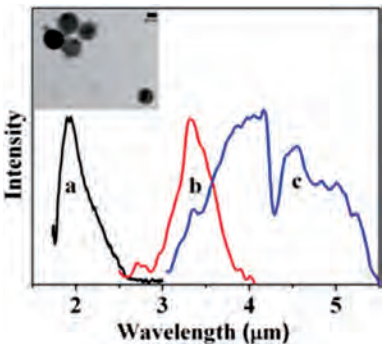

Figure 4 (online color at: www.lpr-journal.org) PL of TM doped II-IV semiconductor nanocrystals. Room temperature PL of a) Cr:ZnS, b) Co:ZnSe, and c) Fe:ZnSe. PL of Fe:ZnSe has a characteristic dip due to atmospheric CO_2 absorption. Insert shows TEM image of 27 nm Cr:ZnS nanoparticles (after [84]).

for electrical-pumping, this thin film technology is of interest for development of waveguide structures, enabling control of optical characteristics in TM^{2+} lasers operating at high powers.

TM doped nano-particles and quantum dots

The majority of methods of metal and semiconductor nanocrystals (NC) synthesis are based on chemical approaches in which a variety of functional groups are used to stabilize NCs and serve as capping agents. Various byproducts of chemical reactions may also interact with NCs and their removal from the surface is tricky. Even small amounts of residual organic molecules used in NC synthesis may reabsorb and/or quench NCs luminescence in the IR region. To resolve this problem the fabrication of the TM doped II–VI nanoparticles by laser ablation was demonstrated in [5, 41]. Initially, TM doped ZnS and ZnSe polycrystalline targets were prepared by thermal-diffusion method. The average TM ions concentration was 10^{18}–10^{19} cm^{-3}. Transition metal doped II–VI NCs were prepared in double distilled and de-ionized water by ablation of solid TM-II–VI targets with a pulsed (30 ps) radiation of the fundamental and third harmonics of Nd:YAG laser. NCs with an average size of 11–13 nm were prepared in aqueous environment by using 1064 nm radiation with 10 mJ pulse energy focused in 2 mm spot. The resulting colloidal suspension was further irradiated by the radiation of the third harmonic (355 nm, 15 mJ, and 1 cm spot diameter) of the same laser in order to produce nanoparticles with an average size of 3 nm. The room temperature PL of Cr, Fe and Co doped ZnSe and ZnS NCs spans over 2–5 μm spectral range as depicted in Fig. 4 [5, 41]. Cr doped II–VI QD technology as proposed in [42] can provide an interesting pathway for future mid-IR tunable solid-state lasers with electrical pumping.

4. Progress in Cr^{2+} doped II–VI lasers

Cr:ZnSe

After the first publication where TM doped II–VI semiconductors were proposed as a new class of solid-state gain media [3], the major attention of researchers was focused on Cr:ZnSe lasers. It was because among all the known Cr doped chalcogenides Cr:ZnSe has one of the most favorable combination of thermal, optical, and spectroscopic properties. A short summary of initial progress in Cr:ZnSe lasers includes: first demonstration of the direct diode excitation [43–45]; CW lasing with efficiency exceeding 60% [45, 46]; gain switched lasing with output power up to 18.5 W [47]; the range of tunability over 1880–3100 nm [48, 49]; active [50] and passive mode-locking [51, 52]; first demonstration of sub 100 fs mode-locked operation [53]; first microchip [54–57] and disk laser [58] operations; single-frequency operation [59]; random lasing [4]; multi-line and ultra-broadband operation in spatially dispersive cavities [60]; lasing via photo-ionization transitions [61]. The minimum laser threshold of 45 mW CW pump power was achieved in [62]. First gain-switched and CW operations of the Cr:ZnSe hot-pressed ceramic samples were demonstrated in [5, 30, 63]. Maximum output characteristics achieved with these samples were reported to be 2 mJ and 250 mW in gain-switched and CW regimes, respectively. Single-frequency CW Cr:ZnSe laser with 150 mW output power was described in [64]. The laser cavity was designed for rapid tunability over 120 nm spectral range centered around 2.5 μm. Tuning rate of up to 4.5 μm/s was demonstrated. Fig. 5 shows a fragment of

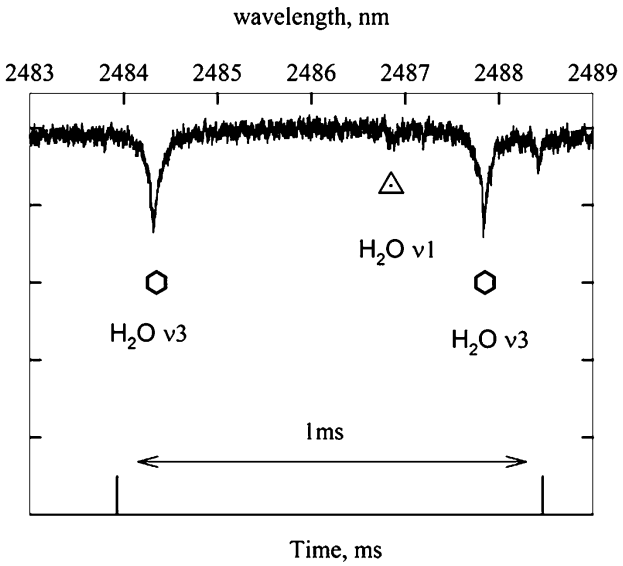

Figure 5 Rapid scanning of the single frequency laser wavelength. Weak vibrational transitions of the v1 and v3 bands of water measured with a single-frequency Cr:ZnSe laser at a scan speed of 4 μm/s.

© 2010 by WILEY-VCH Verlag GmbH & Co. KGaA, Weinheim

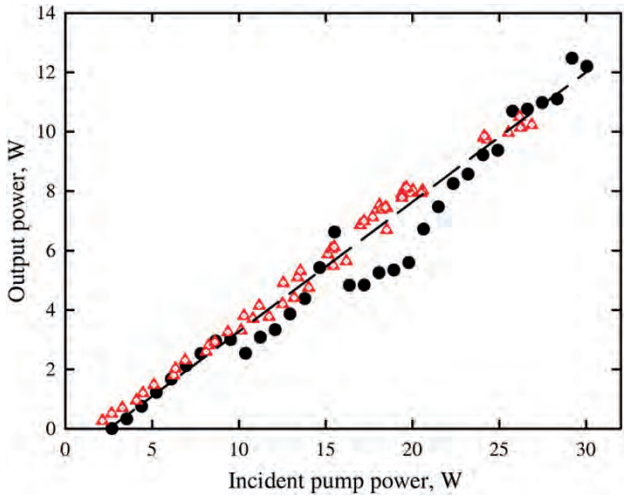

Figure 6 (online color at: www.lpr-journal.org) power vs incident pump power of the Cr:ZnSe (circles) and Cr:ZnS (triangles) lasers. Dashed line represents best linear fit with slope efficiency of ∼43%.

laser tuning curve during fast scanning over 20 nm spectral interval. The intracavity water absorption is responsible for the sharp lines in the signal.

One of the most challenging tasks in power-scaling of Cr^{2+}:ZnSe lasers is thermal lens management. For a long time, the best CW output power result was 1.8 W, reported in 2001 [65]. Recently, authors in several publications demonstrated a significant progress in the developing of high quality Cr:ZnSe crystals and their thermal management [5, 64, 66]. The input-output of the CW Cr:ZnSe shown in Fig. 6 demonstrates about 43% real, and 43.5% slope efficiencies with 12.5 W maximum output power at 29 W incident pump.

Cr:ZnS

In spite of the current overwhelming attention to Cr:ZnSe gain media, the combination of favorable thermo-mechanical, optical, and spectroscopic characteristics of Cr:ZnS crystals indicate that these media can be effectively used in the future for mid-IR lasing. As we have already mentioned, among other chromium doped chalcogenides, Cr:ZnS crystals feature the highest thermal conductivity, the highest level of optical damage, the highest hardness, and the lowest thermal lensing [15]. In addition, absorption and emission bands in Cr:ZnS are ∼100 nm blue shifted in comparison with ZnSe hosts. The first CW operation of Cr^{2+}:ZnS laser with 0.7 W output power was reported in [67]. Gain switched Cr:ZnS laser with 5 ns pulse duration and tuning range of 2050–2400 nm was realized in [68]. The diode pumped operation of the Cr:ZnS laser with threshold pump power of 175 mW was reported in [67]. The first Cr:ZnS laser passively mode-locked by InAs/GaSb SESAM with output power of 125 mW and pulse duration of 1.1 ps was demonstrated in [69]. Multi-watt highly-efficient pure CW Cr:ZnS laser pumped by Er-fiber laser was recently described in [70]. The output-input dependence of the CW Cr:ZnS laser in non-dispersive cavity depicted in Fig. 6 demonstrates the output power in excess of 10 W and slope efficiency as high as 43%. These results clearly indicate that ZnS hosts are very promising for high power mid-IR lasing.

Cr:CdSe

Chromium doped CdSe crystals are very attractive for applications in which direct lasing at wavelengths longer than 3 µm is required. The first room-temperature, broadly tunable laser operation of gain switched Cr:CdSe laser was demonstrated in [71, 72] soon after the first publications on Cr:ZnSe lasers. Output of 500 mW at 2.6 µm with 48% slope efficiency was achieved under Tm:Ho:YLF gain switched excitation with 1-kHz repetition rate and 40 ns pulse duration. For a decade the relatively strong thermal lensing in Cr:CdSe hampered the development of pure CW Cr:CdSe room temperature lasers. The first CW room temperature oscillation of Cr:CdSe was realized only recently in [73], where the authors utilized thin slab geometry gain element and reported an efficient Tm-fiber laser pumped Cr:CdSe laser operating at 2.6 µm with an output power in excess of 1 W and 60% quantum slope efficiency. Among all the known Cr doped chalcogenide lasers, Cr:CdSe features one of the longest ranges of mid-IR tunability. Using 300 µs pump pulses from the free running Tm:YAP laser, the 2.26–3.61 µm tunability of Cr:CdSe laser was achieved in dispersive cavity [74], while in nonselective cavity 17 mJ output energy at 2.6 µm and 63% quantum efficiency were demonstrated.

Other chromium doped II–VI materials

Broadly tunable mid-IR lasing was demonstrated in several other Cr-doped II–VI semiconductors. However, the output characteristics of these laser systems are currently worse than that reported above. The following Chromium doped lasers have been described in the literature: $Cr:Cd_{0.85}Mn_{0.15}Te$ (2.3–2.6 µm) [75], $Cr:Cd_{0:55}Mn_{0:45}Te$ (2.17–3.01 µm) [76], Cr:CdTe (2.54 µm) [77], Cr:CdS (2.2–3.3 µm) [78], $Cr:ZnS_xSe_{1-x}$ (2.1–2.7 µm) [79].

Table 3 summarizes the most important state-of-the-art output characteristics of the Cr:ZnSe, Cr:ZnS, and Cr:CdSe lasers. As one can see Cr doped II–VI lasers could be viable competitors to the conventional semiconductor lasers and laser systems based on frequency conversion techniques. Below we will focus on several non-traditional regimes of oscillation of the Cr^{2+} lasers.

© 2010 by WILEY-VCH Verlag GmbH & Co. KGaA, Weinheim

Table 3 State-of-the-art in Cr and Fe doped II–VI lasers.

Crystal	Laser characteristic	Output parameter	Reference
Cr:ZnS	CW, output power	10 W	[70]
	CW, Tuning range, μm	1.94–2.80	[70]
	CW, efficiency	53%	[55]
	CW, microchip, output power, W	0.1	[55]
	Gain-switched microchip, energy, mJ	0.5	[56]
	Mode-locked, duration, fs	1100 @ 125 mW	[69]
Cr:ZnSe	CW, output power	12 W	[66]
	CW, tuning range, μm	2.0–3.1	[48]
	CW, efficiency, %	60–70	[45,46]
	CW, microchip, output power, W	3	[64]
	CW, hot-pressed ceramic laser, W	0.25	[5]
	CW, single frequency, oscillation linewidth, MHz	20 @ 10 mW < 120 @ 150 mW	[59] [5]
	CW, multiline operation	40 lines over 2.4–2.6 μm	[60]
	Pulsed, output power, W	18.5 @ 10 KHz	[47]
	Pulsed, output energy, mJ	14 @ 200 μs	[109]
	Pulsed, tuning range, μm	1.88–3.10	[49]
	Pulsed Microchip, Energy, mJ	1	[56]
	Gain-switched, hot-pressed ceramic laser, energy, mJ	2 @ 5 ns	[30]
	Mode-locked, duration, fs	80 @ 80 mW	[53]
Cr:CdSe	CW, ouput power, W	1.06 W	[73]
	Pulsed, tuning range, μm	2.26–3.61	[74]
	Pulsed, energy mJ	17@300 μs	[74]
Fe:ZnSe	Pulsed @150 K, energy, μJ	5	[13]
	Pulsed @85 K, energy, mJ	187 @300 μs	[11,85]
	Pulsed, efficiency,%	43	[11,85]
	Microchip gain-switched @300 K, energy, μJ	1 @ 5 ns	[14]
	Gain-switched @300 K, energy, mJ	0.4 @60 ns	[11,86]
	Gain-switched @300 K, tuning range, μm	3.95–5.05	[11,86]
	CW, output power,	150 mW @4.06 μm	[87]

5. Non traditional lasing regimes of the Cr^{2+}-doped II–VI lasers

Microchip and compact lasers

The combination of high $\sigma\tau$ product, high permissible concentration of dopant, and high thermal lensing of the Cr-doped II–VI semiconductors make them ideal candidates for microchip lasing. The first microchip laser experiments on both Cr:ZnS and Cr:ZnSe crystals were performed in [55, 56]. The mirrors were directly deposited on plane-parallel polished facets of 1 mm long Cr:ZnS and 2.5 mm long Cr:ZnSe crystals. Two different pump arrangements were utilized. The first pump arrangement was without any coupling optics and was arranged by microchip laser mounting at a close (∼ 20 μm) distance from the tip of the CW Er-fiber pump laser operating at 1.56 μm. The laser thresholds of 150 mW and 240 mW and slope efficiencies of 36 and 14% with respect to the absorbed pump power were realized for Cr:ZnS and Cr:ZnSe microchip lasers, correspondingly. The second arrangement had focusing optics between the fiber and the microchip. In the focused pump beam arrangement a laser threshold of 120 mW and a slope efficiency of 53% and maximum output power 58 mW were realized for the Cr:ZnS microchip laser. In the case of ZnSe microchip lasing, in the focused pump-beam arrangement a laser threshold of 190 mW with a slope efficiency of 20% with respect to the absorbed pump power was demonstrated.

© 2010 by WILEY-VCH Verlag GmbH & Co. KGaA, Weinheim

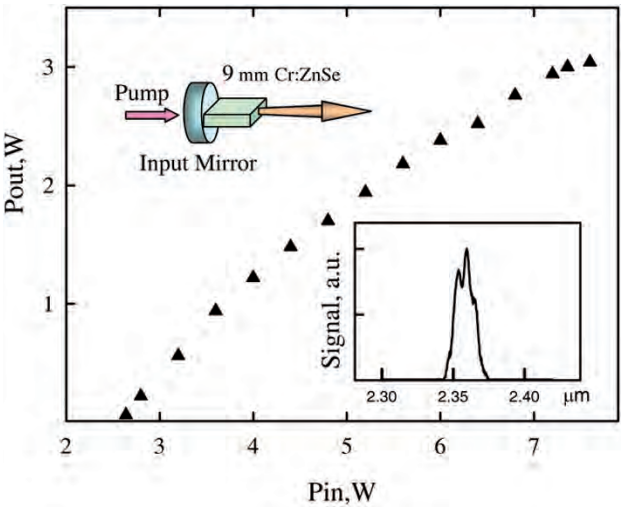

Figure 7 (online color at: www.lpr-journal.org) Output-input dependence of the Er-fiber laser pumped CW compact "microchip" Cr:ZnSe laser. Insert: output spectrum of the "microchip" Cr^{2+}:ZnSe laser.

The output spectra covered the 2280–2350 nm and 2550–2620 nm spectral ranges for ZnS and ZnSe microchip lasers, respectively. Maximum output power of the Cr^{2+}:ZnSe microchip laser was reported to be 0.5 W [5]. The ultra-compact Cr:ZnSe laser consisted of only two elements: a flat input mirror and uncoated, rectangular, plane-parallel, 9 mm Cr:ZnSe crystal was reported in [64]. The output facet of the gain element served as a 17% output coupler. The output characteristics of this ultra-compact laser are depicted in Fig. 7. The laser operates around 2.4 μm and delivers up to 3 W of output power at about 7.5 W pump with 59% slope and 41% real optical efficiencies, and generates 20 nm broadband output spectrum. Gain switched microchip lasing was demonstrated using uncoated ZnSe and ZnS crystals with laser cavity formed by Fresnel reflections [57]. The best results were obtained using 5.5 mm Cr:ZnSe crystal with Cr concentration 6×10^{18} cm^{-3}. The threshold pump energy was found to be 7 mJ. The maximum slope efficiency of 6% and maximum output energy of 1 mJ were obtained.

Lasing in the spatially dispersive cavities

Cr:ZnSe crystal dual-wavelength lasing, as well as multi-line, and broadband lasing have been demonstrated in a spatially-dispersive cavity [60]. The cavity design of this laser system provides spatial separation of different oscillation wavelengths in the gain media. It results in the elimination of competition among oscillation modes with different wavelengths. The described spatially-dispersive laser can operate at many wavelengths simultaneously producing any pre-assigned output spectral composition as well as a continuous ultra-broadband spectrum within the emission band of the gain medium. The Er-fiber laser pumped, dual-wavelength, CW Cr:ZnSe laser spectral output is depicted in Fig. 8. The simultaneous tuning of the output wavelengths is shown in Fig. 8 where two wavelengths, separated by 50 nm, are tuned over a 600 nm spectral range. The individual tuning of the spectral lines in the dual-wavelength mode of operation is shown in Fig. 8. In this case the wavelengths are tuned separately so that the wavelength separation is consequently changed from 30 to 560 nm. Multi-wavelength or ultra-broadband laser output can be obtained in the single dispersive cavity using specific spatial shape of the pumping beam. Simultaneous tuning of a 40-line ultra-broadband spectrum over a spectral range of 2200–2800 nm was reported in [60]. These lasers could find important practical application for free space optical communication, information coding, remote sensing, and numerous wavelength specific military applications.

Random lasers in the powder, colloidal solution and polymer films

The idea of the random laser with positive feedback resulting from multiple scattering in the gain medium was suggested in 1966 by Letokhov [80]. The most probable application for these lasers is spectral coding including long-range rescue and military identification of friend and foe [33]. This application requires low-cost, low laser threshold, and a widely tunable laser medium. Recent development of the TM doped II–VI laser powder fabricated

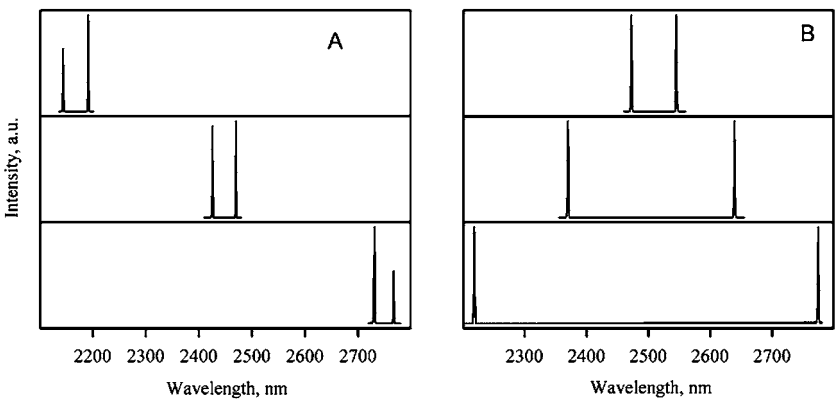

Figure 8 Wavelength tuning of spatially-dispersive CW Cr:ZnSe laser operating in dual-wavelength regime. (A) Simultaneous tuning of two lasing lines. (B) Independent tuning of two lasing lines (after [5]).

© 2010 by WILEY-VCH Verlag GmbH & Co. KGaA, Weinheim

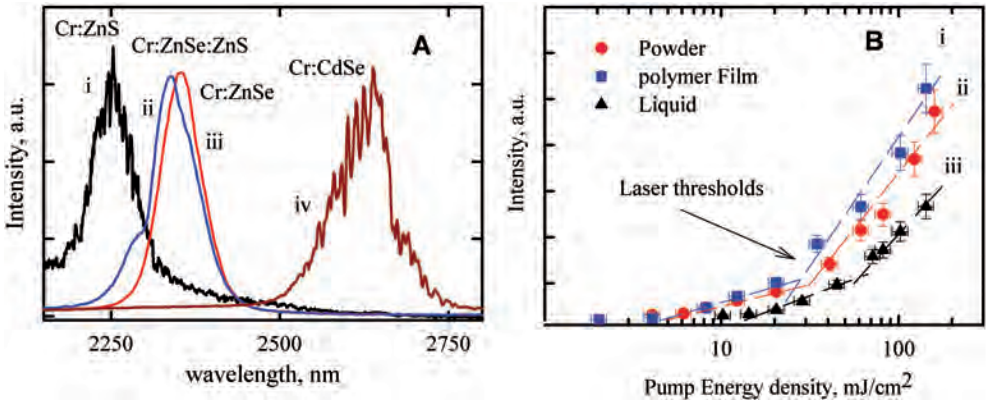

Figure 9 (online color at: www.lpr-journal.org) A) RT random lasing spectra of Cr-doped powders: (i)-Cr:ZnS; (ii)-Mixed Cr:ZnSe/Cr:ZnS; (iii)-Cr:ZnSe; and (iv)-Cr:CdSe. B) RT output emission intensity versus pump energy density for Cr^{2+}:ZnSe powder in (i) polymer film, (ii) powder, and (iii) liquid solution.

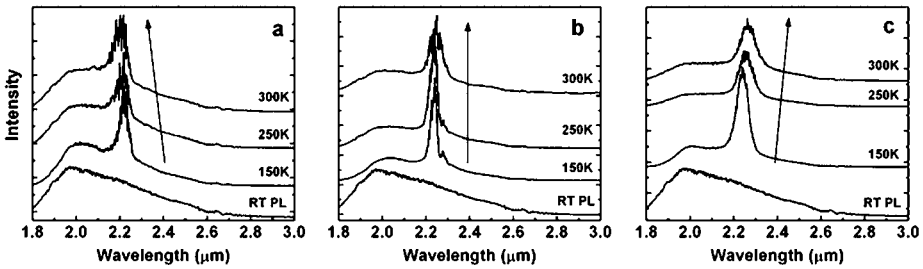

Figure 10 Temperature and size dependence of Cr:ZnS NCs lasing. Lasing emission at different temperatures of samples prepared from a) 27 nm NCS, b) 250 nm NCs, and c) 3 μm particles. RT emission spectra (below laser threshold) of the Cr:ZnS NCs are shown at the bottom.

without bulk crystal growth stage [31, 32] can enable practical realization of these applications. In these experiments, 1–10 μm grain size powder was placed on a glass slide or in a glass tube with an inner diameter 5 mm. Pump beam from an optical parametric oscillator at 1.9–1.7 μm wavelength and 5 ns pulse duration was slightly focused on the powder. Fig. 9 shows typical oscillation spectra of several Cr doped II–VI powders. Changing powder composition and grain size one can tune Cr random laser over 2240–2630 nm spectral range. The typical lasing spectral widths were ∼ 70 nm. However, adding absorbing powders to the mixture could narrow the lasing line. The Cr doped II–VI powder maintains laser properties both in the polymer film and liquid solution transparent in the IR spectral range. Fig. 9 demonstrates typical threshold-like behavior of the random lasing output for Cr doped ZnSe powder (1), film (2), and liquid solution (3). The minimum threshold of the pump energy density was reported for 10 μm size powder and was as low as 7.4 mJ/cm^2. Lasing threshold of the powders prepared by chemical component annealing was 6 times smaller than lasing threshold of the powders prepared by mechanical grinding of bulk crystal [79].

TM doped quantum dots lasers

Recently developed fabrication methods for TM-doped II–VI NCs [5, 41] allow preparation of powders with different grain sizes from 3 nm to dozens of microns. This technology can address several fundamental physical problems. In recent years, there has been a growing interest in photon localization in the disordered systems (Anderson localization) resulting from multiple elastic scattering [81]. The Ioffe–Regel condition $k \cdot l_s \sim 1$ (where k wave vector and l_s the transport mean free path) is the key criteria for such localization. To the best of our knowledge, minimal mean free path was reported $l_s \approx 0.17$ μm at 1.06 μm for GaAs powder which corresponds to $k \cdot l_s \sim 1.5$ [82]. The measured mean free path in the 27 nm Cr:ZnS NCs was equal to 648 nm at 632 nm wavelengths which corresponds $k \cdot l_s \sim 10$ [83]. These results demonstrate that Chromium doped II–VI laser active NCs are proper materials for phonon transport studies in the disordered media. Besides, TM doped semiconductors are good candidates for future electrically pumped mid-IR TM lasers. Understanding the mechanisms of energy transfer from the carriers to the deep level TM impurities is the key problem for realization of this goal. Quantum confinement could be the major factor enhancing this process. First RT mid-IR lasing due to impurity intra-shell transitions in the TM doped semiconductor nano-crystals was reported in [83]. Laser experiments with nano-sized and micro-sized powders were performed in the mirror-less random lasing regime using 10 ns pump pulses at 1.7 μm. Fig. 10 shows typical laser spectral spikes for different samples prepared from 27 nm, 250 nm, and 3 μm Cr:ZnS particles. The temperature dependence of the lasing wavelength reveals different behavior for different NC's particles. Lasing wavelength of 27 nm NCs with temperature rise is shifted to the shorter wavelength, while large particles demonstrate red shift with temperature rise. Detailed studies explain this behavior by different scattering regimes in the samples [84]. In the case of small (27 nm) NCs, the laser feedback is stronger for shorter wavelengths due to increase of scattering efficiency

© 2010 by WILEY-VCH Verlag GmbH & Co. KGaA, Weinheim

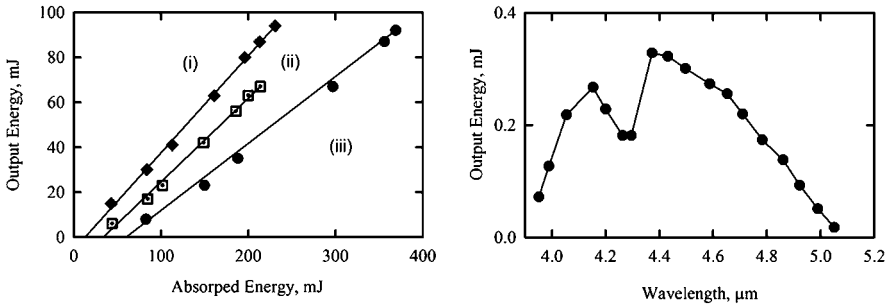

Figure 11 A) Input-Output characteristics of Fe^{2+}:ZnSe laser at different temperatures of the active elements (i – 85 K; ii – 186 K; iii – 220 K obtained with thermoelectric cooler). B) Tuning curve of room-temperature Fe^{2+}:ZnSe laser with intracavity prism obtained at absorbed pump energy of 4.5 mJ (after [11]).

(Raleigh scattering regime). On the contrary, scattering in the other samples was located in the Mie region, since the size of scatters was comparable with radiation wavelength. Scattering mean free path of the samples made from big particles is less spectral sensitive. Therefore, lasing spectra shift to the red region following the temperature change of the gain media.

6. Progress in Fe^{2+} doped II–VI lasers

Temperature quenching of the mid-IR luminescence in the iron doped II–VI chalcogenides was one of the reasons why these gain media were considered less promising for RT mid-IR lasing. In addition, the position of the absorption band is around 3–3.5 μm wavelength where the number of the available pump sources is very limited. As a result, to the best of our knowledge, the laser oscillation of Fe^{2+} ions was reported only for ZnSe host. First low temperature Fe:ZnSe lasing was achieved for temperature ranging over 15–180 K [13]. Using free-running Er:YAG laser at 2.7 μm the authors demonstrated 12 μJ lasing energy at 4.5 μm. The next significant progress was demonstrated in [85]. The authors studied laser characteristics of the low doped (10^{18} cm^3) Fe:ZnSe crystal in the 85–255 K temperature range using 2.9 μm free running Er:YAG pump laser. In this research, the authors demonstrated two important issues. As one can see from Fig. 11, they showed 43% (at $T = 85$ K) slope efficiency with output energy 91 mJ at 4.0 μm. It demonstrated the feasibility of a Fe:ZnSe laser system with output energy sufficient for many practical applications. The second important issue was Fe:ZnSe lasing with thermo-electrical cooling. Using two-stage thermoelectric cooling, the maximum output energy and slope efficiency at $T = 220$ K were reported to be 160 mJ and 23% correspondingly. These results are especially important for practical application of the Fe:ZnSe lasers since they make it possible to avoid cryogenic temperatures and instead design practical thermo-electric cooled system.

The next important step in the development of Fe:ZnSe lasers was realized in [14]. Based on spectroscopic characterization and direct lasing experiments, the authors demonstrated that in spite of non-radiative quenching at RT, Fe:ZnSe crystals have a big emission cross-section, 370 ns excited-level lifetime, and can be used for RT lasing in the gain-switched regime. Moreover, the stimulated emission was observed at RT without any coatings on crystal surfaces when oscillation feedback resulted from only Fresnel reflections on crystal surfaces ($R \sim 17\%$) [14]. Pump source for these laser experiments was the 2nd Stokes output (2.92 μm) of the Nd:YAG laser in a D_2 cell with 5 ns pulse duration. The laser threshold was measured to be 50 mJ/cm^2 for 2 mm Fe:ZnSe crystal with iron concentration 6–9$\times 10^{18}$ cm^3. The laser spectral line was centered at 4.35 μm with a linewidth of 0.15 μm. The maximum output energy was estimated to be ~ 1 μJ. After the first publication, the efficient RT Fe:ZnSe laser oscillation was achieved using 2.94-μm passively Q-switched Er:YAG laser as a pump source [11]. It is noteworthy, that for these experiments the passive Q-switching of the Er:YAG laser was realized using Fe:ZnSe crystal. The threshold pump energy of the Q-switched Er:YAG laser was 19 J. Under pump energy $E = 19$–21 J the laser produced a single 6.5-mJ, 50-ns (FWHM) giant pulse. The input-output characteristics of the room temperature Fe:ZnSe lasing are shown in Fig. 11. Laser oscillation at 4.4 μm was obtained with maximum output energy of 0.37 mJ and slope efficiency of 13%. The delay between pump and oscillation pulses was 20–30 ns; the Fe:ZnSe laser pulse duration did not exceed 40 ns.

Tunable oscillation of the Fe:ZnSe was demonstrated with diffraction grating in the Littrow cavity [14] and with a CaF_2 dispersive prism [11,86]. The achieved tuning curve shown in Fig. 11 covers the spectral range 3.95–5.05 μm and on the short-wavelength edge is probably limited by the output coupler reflectivity. Also, as one can see from Fig. 11, the measured tuning curve has a deep dip around 4300 nm due to atmospheric absorption of CO_2.

To the best of our knowledge, there is only one conference presentation [87] where CW operation of the Fe:ZnSe laser was reported. The authors reported 160 mW CW Fe:ZnSe lasing at 4.06 μm with 56% slope efficiency. A CW Cr:CdSe laser operating at 2.97 μm was used as a pump source.

7. Electrical excitation of the transition metals in semiconductors

In addition to effective RT mid-IR lasing transition metal doped II–VI media, being wide band semiconductors, hold

© 2010 by WILEY-VCH Verlag GmbH & Co. KGaA, Weinheim

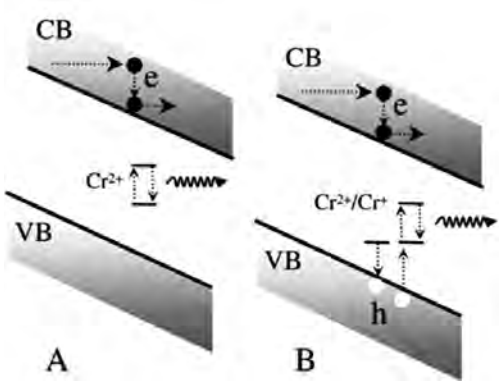

Figure 12 Impact excitation (A) and impact ionization (B) mechanism of Cr^{2+} ions in II–VI crystals.

potential for direct electrical excitation. Possibility of electrical pumping of mid-IR semiconductor lasers based on TM doped II–VI structures was investigated in several publications [34,41,88–90]. This new type of laser could possess some advantages in comparison with other mid-IR laser sources such as quantum cascade lasers; semiconductor diodes (InAsSbP/InAsSb/InAs), and systems based on nonlinear frequency conversions (optical parametric oscillation and difference frequency generation). In comparison with semiconductor lasers, TM:II–VI has significantly broader tuning range; and in comparison with nonlinear devices they could be considerably less expensive and bulky. In addition to II–VI materials, the electroluminescence of Fe^{2+} in the III–V semiconductors was reported in several publications. A review of these studies can be found in [91]. However, electrically pumped mid-IR lasers based on TM doped semiconductors have not been documented in the literature.

For successful realization of electrical excitation two conditions should be satisfied: (i) effective and sustainable excitation of the crystal host by electrical current; and (ii) effective energy transfer from the host to the mid-IR lasing TM impurity. The feasibility of the first condition is supported by the results reported in [92] on development of II–VI visible LED sources operating with a lifetime exceeding 10,000 hours. The second condition can be achieved either via carrier impact energy transfer or via recombination processes in bulk and especially in quantum confined structures.

TM ions excitation mechanisms as a result of carrier-TM ions impact interaction have been studied for many decades. These mechanisms are dominant in high-field driven electro-luminescence devices including Mn:ZnSe structures described as early as 1960 by Vlasenko and Popkov [93]. In these structures, after reaching electric field threshold, the electron energy can be transferred to TM impurities. In the Mn doped II–VI materials, these processes are followed by intra-shell $^4T_1$–$^6A_1$ radiative transition in the yellow-orange spectrum range. Fig. 12 shows two possible mechanisms by which electrons can excite deep-level TM impurity ions (Cr^{2+} in our case). In the impact excitation process the energy (Fig. 12A) of an electron is transferred directly to the impurity. This process requires electron energy of ~ 0.6 eV for ^5E-$^5T_2$ excitation of the Cr^{2+} ions. The second mechanism (Fig. 12B) involves ionization of the Cr^{2+} ions and needs an additional carrier capture to provide Cr^{2+} in the excited state. This process must have higher kinetic energies of carriers with respect to collision impact excitation (Fig. 12A). The ionization energy for the $Cr^{2+} \rightarrow Cr^{+}$ process in the ZnS crystal has been measured using photo-induced ESR and was estimated to be ~ 2.3 eV [94]. The basic advantage of these impact energy transfer mechanisms is the simplicity of sample preparation. The obvious shortcomings are: a) the necessity of using a high electric field of 0.1–1 MV/cm [95] for wide band semiconductor devices, and b) low efficiency of energy transfer, since most of the electrons cross the active layer without impacting any TM ions [96].

Direct impact excitation and impact ionization of the TM ions by hot electrons has been studied for many years [97] and, specifically for wideband semiconductors, the impact excitation processes were most closely scrutinized for the EL Mn:ZnS devices. The alternate current (AC) driven EL displays based on Mn:ZnS material with an operating lifetime of more than 50,000 h were developed several years ago [95]. The impact excitation efficiency can be expressed in terms of a fraction of the excited impurity ion (f) concentration. This fraction can be estimated using the lucky-drift model [97]. According to [96] the fraction of the excited TM ions (f) under pulsed electrical excitation can be calculated as

$$f = (\Delta Q/e)\,\sigma_{12}\,(v_g\,/\,v_d)\cdot\exp\left(-E_m\,/\,eF\lambda_E\right), \qquad (2)$$

where ΔQ – internal transferred charge; λ_E – energy relaxation length; E_m – ionization energy parameter; F – electric field; e – elementary charge; v_g, v_d – group and drift carrier velocities, respectively.

In the experimental studies of the Mn:ZnS high field EL devices the fraction (f) was estimated to be $\sim 10^{-2}$ [95] with parameter $\Delta Q/e \approx 5\times 10^{13}\,\mathrm{cm}^{-2}$. Based on Eq. (2), one can estimate the required inversion parameter (f) for the lasing threshold in Cr:ZnSe samples. In [62] the minimum threshold pump-power was reported to be 45 mW @ 1.6 μm for 1% transmission of output coupler, and 80×80 μm beam spot size ($W_{\mathrm{th}} \approx 0.7\,\mathrm{kW/cm}^2$). Taking into account the Cr:ZnSe saturation intensity $W_s = \hbar\omega/\sigma_p\tau \approx 55\,\mathrm{kW/cm}^2$ ($\sigma_p = 4.4\times 10^{-19}\,\mathrm{cm}^2$, $\tau = 5.5\,\mu\mathrm{s}$), the inversion parameter at the laser threshold in this experiment was equal to $f = W_{\mathrm{th}}/W_s \approx 1\%$. A similar value for the required inversion parameter ($f \sim 1\%$) at the laser threshold is obtained from the optical gain-loss balance. Indeed, for common 3% single-pass passive optical losses in 0.2 cm long Cr:ZnSe crystals [62] with chromium concentration $N_{\mathrm{cr}} = 10^{19}\,\mathrm{cm}^{-3}$, the inversion parameter f is estimated to be approximately 0.01: $f = \ln G/N_{Cr}\sigma_{\mathrm{em}}L \approx 0.01$. Thus we find that Cr^{2+} mid-IR threshold population inversion is of the same order of magnitude as that already achieved for Mn^{2+} under high field electrical excitation. In com-

© 2010 by WILEY-VCH Verlag GmbH & Co. KGaA, Weinheim

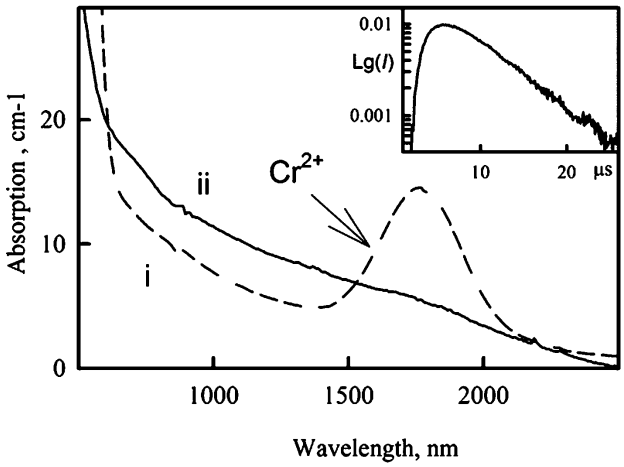

Figure 13 Absorption spectra of Cr:ZnSe crystal before (dashed line) and after (solid line) Ag co-doping. Insert shows kinetics of Cr^{2+} ions mid-IR luminescence excited by 532 nm light via ionization transition.

parison with high energy (~ 3 eV) quanta of Mn^{2+} visible electro-luminescence, Cr^{2+} has significantly smaller energy splitting between ^{2}T and ^{2}E levels (~ 0.6 eV) and smaller ionization energy (~ 2.3 eV). In addition, unlike $^4T_1$–$^6A_1$ Mn^{2+} transitions, the chromium transitions $^2T \leftrightarrow {}^2E$ are spin allowed. Overall, the combination of these factors should result in a higher excitation rate of Cr^{2+} ions for identical electrical excitation conditions.

Electroluminescence of the n-type Cr:Al:ZnSe and p-type Cr:Ag:ZnSe bulk samples was studied in the visible, near- and mid-IR spectral regions under DC electrical excitation [89, 98]. The n-and p-type samples were obtained by subsequent diffusion of Al or Ag powders in the Cr:ZnSe crystals. Initially, Cr^{2+} concentrations in the ZnSe samples were $5–15 \times 10^{18}$ cm^{-3}. One of the challenges in developing II–VI conductive structures is related to self-compensation processes when carrier trapping by native host defects or residual impurities limits conductivity, especially in p-type ZnSe. Presence of the deep-level Cr impurities even aggravates the problem. In all cases Cr doped samples showed poorer conductivity than similar prepared samples without chromium impurities. In addition, the reduction of the Cr^{2+} concentration was observed during the co-doping procedure. One of the reasons of the Cr^{2+} suppression could be the valence change of Cr^{2+} ions in the chromium-donor/acceptor complexes (like Cr^{+}-Ag^{+}). In most cases good conductivity was observed only after total Cr^{2+} compensation. Fig. 13 shows absorption spectra of the Ag:Cr:ZnSe sample before and after annealing. As one can see, the Ag co-doping results in diminishing of the Cr^{2+} absorption band at the $^5E \leftrightarrow {}^5T_2$ transition. Similarly, Al co-doping was accompanied by a $\sim$two-fold decrease of the Cr^{2+} coefficient of absorption in the Al:Cr:ZnSe crystals. It is noteworthy, that in spite of the absence Cr^{2+} absorption in the Ag:Cr:ZnSe sample, the mid-IR $^5E \leftrightarrow {}^5T_2$ photoluminescence of Cr^{2+} was observed under ionization transition stimulated by 532 nm excitation. The PL kinetics, shown in the insert to Fig. 13, reveal a rise-time of several μs caused by the relaxation process from the high-lying levels of the Cr^{2+} to the upper 5E level. The PL rise was followed by radiative decay with 7 μs lifetime. This decay time is clear evidence of the absence of the quenching mechanisms of the mid-IR photoluminescence in the Ag co-doped crystals.

The conductivity of the crystals was verified by I–V measurements and shown in Fig. 14. Before the co-doping procedure the Cr:ZnSe sample had a high resistivity $\rho > 10^{10}\ \Omega$·cm. After co-doping the resistivity of the Al:Cr:ZnSe samples was ($\rho = 84\ \mathrm{k}\Omega$·cm) higher than in Ag:Cr:ZnSe crystal ($\rho = 600\ \Omega$·cm). Mid-IR electroluminescence of the Cr:Al:ZnSe and Ag:Cr:ZnSe samples was studied under pulse electrical excitation with pulse duration ranging from micro- to milliseconds. Fig. 15 shows the mid-IR electroluminescence signal of the Al:Cr:ZnSe and Ag:Cr:ZnSe samples detected by InSb detector with 2–3 μm bandpass filter. The mid-IR electroluminescence spectrum of Cr:Al:ZnSe is depicted in Fig. 15 curve iii. As one can clearly see the Cr:Al:ZnSe electroluminescence is in good agreement with PL of the same sample measured under direct optical $^5T_2 \leftrightarrow {}^5E$ excitation. It was also revealed that under electrical excitation, in addition to Cr^{2+} mid-IR electroluminescence, there exist luminescence signals in two other spectral bands: a strong visible emission band detected near 600 nm and a luminescence band around 8 μm. The nature of this electroluminescence requires additional study. In recent publications authors [99–101] demonstrated

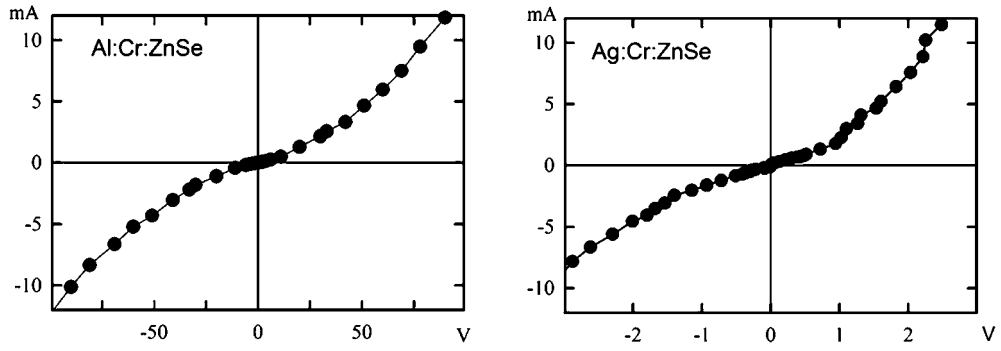

Figure 14 Conductivity measurements of Al:Cr:ZnSe and Ag:Cr:ZnSe crystals.

© 2010 by WILEY-VCH Verlag GmbH & Co. KGaA, Weinheim

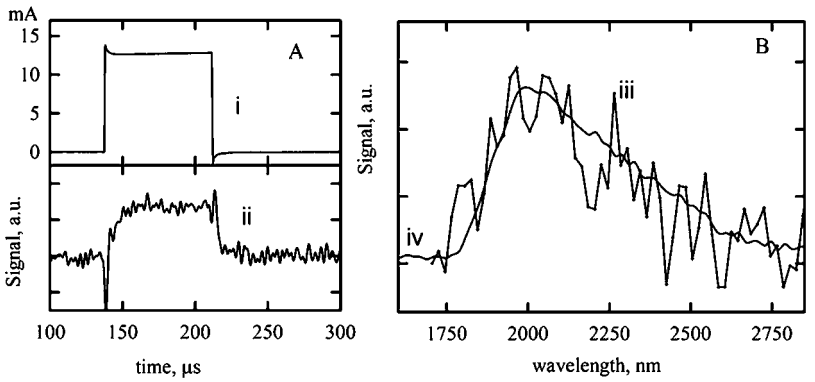

Figure 15 A) Oscilloscope traces of the electrical current across the Al:Cr:ZnSe sample (i) and the mid IR optical signal (ii). B) Mid-IR electroluminescence (iii) and photoluminescence (iv) of the Cr^{2+} ions in the ZnSe sample.

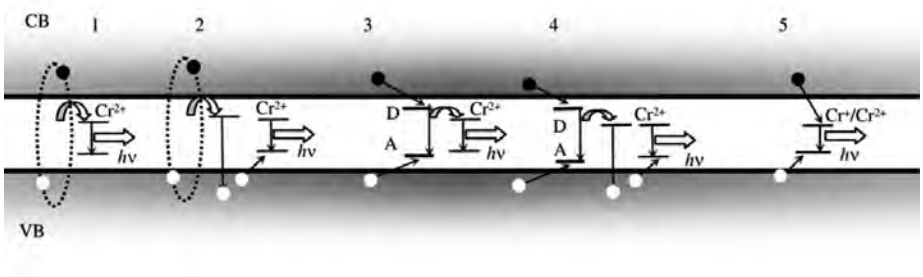

Figure 16 Major mechanisms of inter-band excitation of intra-shell mid-IR emission of Cr^{2+} ions via i) energy transfer from the bound exciton (1) and from adjacent DAP (3); ii) TM^{2+} ionization caused by Auger-type recombination processes (2,4); and iii) carrier trapping by TM impurity (5).

electroluminescence in the Cr:ZnS(Se) thin-film structure under AC excitation (ACTFEL). The strong increase of the Cr^{2+} emission intensity proportional to Q^6 was reported in [102], where Q is the charge transferred through the EL film for the applied voltage cycle.

Excitation via recombination processes

Most disadvantages of high-field devices (such as low efficiency and operation near electrical breakdown) can be avoided in the structures with carrier recombination. In these structures, the released energy is large enough (order of band-gap); therefore, there is no requirement for a high electric field application to the structure. It was found that the recombination energy transfer for mid-IR intra-shell photoluminescence of Cr could be described by the following major mechanisms [94, 103–105]:

a) The first process (Fig. 16-1) relates to the non-radiative energy transfer from the excitons to the high lying levels of the transition metal. A similar process could also result in Auger-type ionization of the TM^{2+} ions followed by carrier capture, formation of excited TM^{2+*} ions, their intra-shell relaxation to the TM^{2+} upper laser level, and finally radiative mid-IR transition to the ground state closes the cycle (Fig. 16-2).
b) The second process (see Fig. 16-3) relates to TM excitation caused by energy transfer from the adjacent donor-acceptor pair (DAP) to the TM ion leading to TM intra-shell excitation. This energy transfer process (see Fig. 16-4) also could result in TM^{2+} ionization, followed (like in process 16-2) by carrier capture, formation of excited TM^{2+*} ions, their intra-shell relaxation to the TM^{2+} upper laser level, and finally radiative mid-IR transition to the ground state will closes cycle.
c) The third process (see Fig. 16-5) relates to the carrier trapping by ionized impurity followed by intra-shell relaxation to the TM^{2+} upper laser level and intra-shell emission of the TM ion.

The variety of the above summarized excitation processes clearly shows that Cr is an exceedingly active center of interband recombination leading to intracenter excitation and mid-IR emission. Hence, it is of significant importance to study in detail the nature of the physical mechanisms of Cr^{2+} ions excitation, to identify the most effective mechanisms and to formulate conditions necessary for realization of electrical-pumping excitation-rate sufficient for achieving mid-IR lasing.

To the best of our knowledge there are no publications on Cr^{2+} lasing under electrical excitation. However, there are experimental results demonstrating feasibility of the Cr:ZnSe lasing under electrical excitation via injected carrier recombination [41, 90] as well as similar carrier processes (via photo-ionization transitions) induced by visible optical excitation [41, 90]. Furthermore, as described in the next paragraph, the efficiency of energy transfer from the host to the lasing impurity is expected to increase in TM doped II–VI quantum confined structures.

Peculiarities of Cr^{2+} excitation in quantum confined II–VI structures

There are numerous publications describing preparation, luminescence properties and potential applications of

© 2010 by WILEY-VCH Verlag GmbH & Co. KGaA, Weinheim

Mn^{2+}:II–VI nanoparticles. The interest in this phosphor was stimulated by Bhargava [106] whose most fundamentally interesting result was luminescence enhancement resulting from efficient energy transfer from the ZnS nanocrystals to Mn^{2+} ions facilitated by mixed electronic states. However, the photo-physical properties of Cr doped II–VI QDs have not been addressed yet. It is believed that, similarly to Mn doped ZnS nanocrystals, one can expect an efficient energy transfer from the low dimensional II–VI structures to Cr^{2+}. Fast energy transfer from the low-dimensional host to Cr^{2+} can be qualitatively explained by the increase of the exciton oscillator strength bound to the impurity center. First of all, quantum size confinement should increase the oscillator strength of the free exciton due to the increase of the electron-hole overlap factor. Secondly, the exciton oscillator strength bound to the impurity center depends on the oscillator strength of the free exciton and electron-hole exchange interaction term which is also supposed to be large due to the carrier's confinement. Thus, we may expect a large enhancement of the oscillator strength of the exciton bound to the impurity embedded in nanostructured materials with respect to bulk hosts. Another experimental evidence of efficient energy transfer from the ZnS QD host (2 nm size) to the TM impurity was reported in [107]. It was demonstrated that, even at small concentrations of Ni ($\sim 0.01\%$), the intensity of the visible near band-gap luminescence of QSs experienced a 4-fold decrease compared to un-doped samples. This blue light emission in ZnS QD was completely quenched when doped with higher iron or nickel metal concentration. It was demonstrated in [108] that the fluorescence intensity of Ni^{2+} doped ZnS QDs due to the d–d optical transitions of Ni^{2+} ions was much higher than near band-gap luminescence of pure ZnS nanocrystals. It is another clear demonstration of the effective energy transfer from the carrier recombination process to the transition ions in the QDs. Recombination processes in 2D CdTe structures containing Cr ions were studied in [103], where shortening of kinetic decay time of the excitonic PL in the Cr doped samples was reported. The authors observed that decay time reduced from 490–320 ps (in CdTe QW structures) to 200–75 ps for CdCrTe QWs structures. The shortest PL decay time was observed for QW with the highest Cr concentration. These results demonstrate that in the QW structures efficiency of the energy transfer to the Cr ions could be significantly improved in comparison with hetero-junction structures. This analysis provides a background for the remarkable differences that could be expected in excitation of Cr^{2+} ions in nanostructures with respect to the bulk crystals and motivation for studies of these nanostructures.

Conclusions

TM doped II–VI chalcogenides, being close mid-IR analogs of the titanium-doped sapphire in terms of spectroscopic and laser characteristics, are capable of lasing in the mid-IR with a great variety of possible modes of oscillation. The unique blend of material (low phonon cut-off, broad IR transparency, high thermal conductivity), spectroscopic (ultrabroadband gain bandwidth, high $\sigma\tau$ product, high absorption coefficients, reasonably high quantum efficiency at RT), and technological parameters (low-cost, mass production technology of crystal fabrication by post-growth thermal diffusion of impurities), as well as the availability of a number of convenient pump sources (InGaAsP/InP diode lasers and diode arrays, Er- and Tm-fiber lasers) make these materials ideal candidates for broadly tunable mid-IR lasing in CW, gain-switched, mode-locked, and microchip regimes of operation. This review summarizes experimental results on optically pumped RT lasers based on Cr:ZnS, Cr:ZnSe, Cr:$Cd_{1-x}Mn_xTe$, and Cr:CdSe crystals providing access to the 1.9–3.6 µm spectral range with high (up to 70%) efficiency, multi-Watt-level (18 W in gain switch and 13 W in pure CW) output powers, tunability in excess of 1000 nm, and narrow spectral linewidth (< 20 MHz). Cr:II–VI lasers have really came of age and, arguably, represent nowadays the simplest and the most cost-effective route for high power, broadly tunable RT lasing over 1.9–3.6 µm.

In addition to Cr based chalcogenides, the article describes emerging Fe^{2+}:ZnSe gain materials having the potential to operate at room temperature over the spectral range extended to 3.7–5.1 µm. Recent progress has demonstrated that Fe^{2+}:ZnSe lasers can operate in gain-switched regime at RT with efficiencies of dozens of percents generating output energies from mJ level at RT till hundreds of mJ with thermo-electric cooling of the crystal.

Future progress of Cr- and Fe-doped II–VI lasers in terms of extending spectral coverage over 3–4 µm and 5–6 µm depends on the search for new, low-phonon-cutoff Cr- and Fe-doped binary and ternary II–VI semiconductor bulk materials. Future improvements in hot-pressed ceramic chalcogenides can stimulate affordable mass production and allow engineering of the laser elements with high optical quality (undoped ends, waveguiding structures, gradient of dopant concentration, etc). These technological steps are immensely important for the development of efficient, high performance chip-scale-integrated lasers as well as lasers with output power and energy scaled-up, respectively, to hundreds of Watts and several Joules.

In addition to effective RT mid-IR lasing transition metal doped II–VI media, being wide band semiconductors, hold potential for direct electrical excitation. This work reviews different mechanisms of TM ions electrical excitation in II–VI crystals via carrier impact, carrier impact ionization, and carriers' recombination. Analysis shows that, even for less effective impact excitation and impact ionization of the TM ions by hot electrons, high electric field TM:II–VI laser structures are feasible, while carrier recombination in p-n and especially in quantum confined structures can significantly improve the efficiency of energy transfer from the electrically excited host to lasing TM impurity. This review also shows the initial steps towards achieving this goal by studying electroluminescence in bulk Cr:ZnSe and as well as Cr^{2+}, Co, and Fe doped laser active nanocrystals. We have demonstrated a novel method of TM doped II–VI

© 2010 by WILEY-VCH Verlag GmbH & Co. KGaA, Weinheim

nanocrystals fabrication based on laser ablation in a liquid environment. This technique has a considerable advantage over chemical synthesis of doped II–VI NCDs due to the possibility of doping nanocrystals with a variety of TM ions using laser ablation of thermo-diffusion doped polycrystalline II–VI targets. For the first time to our knowledge TM doped II–VI nanocrystals demonstrated strong mid-IR luminescence and random lasing. It opens a new pathway for future optically and electrically pumped mid-IR lasers based on TM doped quantum confined structures.

Acknowledgements The authors would like to thank Andrew Gallian for help with experiments. We are also grateful to our colleagues and collaborators K. Schepler, P. Berry (AFRL), M. Mirov (Photonics Innovations, Inc.), V. Gapontsev, D. Gapontsev, N. Platonov (IPG Photonics Corporation), V. Badikov and D. Badikov (Kuban State University, Russia), E. Dianov and A. Zabezhailov (General Physics Institute, Russian Academy of Sciences), I. Kazakov, M. P. Frolov, Y. V. Korostelin, V. I. Kozlovsky, A. I. Landman, Y. P. Podmar'kov, V. A. Akimov, A. A. Voronov (P. N. Lebedev Physics Institute, Russian Academy of Sciences), I. Sorokina (Norwegian University of Science and Technology) and E. Sorokin (Vienna University of Technology).

This material is based upon work supported by the National Science Foundation under Grants No. ECS-0424310, BES-0521036, EPS-0447675, and EPS-0814103.

Sergey B. Mirov was born in Moscow, Russia on December 4, 1955. He received the M. S. degree in electronic engineering, from the Moscow Power Engineering Institute – Technical University, in 1978, and the PhD degree in physics, from the P. N Lebedev Physical Institute of the Russian Academy of Sciences, Moscow, for his work on tunable color center lasers. He served as a staff research physicist, at P. N. Lebedev Physical Institute, and a principal research scientist and a group leader at the General Physics Institute of the Russian Academy of Sciences. His early work in Russian Academy of Sciences involved physics of color centers formation under ionizing irradiation, color center's photo chemistry, laser spectroscopy of solids and led to the development of the first room temperature operable commercial color center lasers, passive Q-switches and nonlinear filters for various types of neodymium lasers from mini lasers to powerful laser glass systems. He was awarded the USSR First National Prize for Young Scientists, in 1982, for the development of LiF color center saturable absorbers. He received Distinguished Research Awards from the General Physics Institute, in 1985 and 1989, and from the P. N. Lebedev Physical Institute in 1980. Since 1993 Dr. Mirov is a faculty member at the Department of Physics of the University of Alabama at Birmingham (UAB), USA. Currently, he is a professor of physics at the UAB and co-director of the Center for Optical Sensors and Spectroscopies. His main fields of interest include tunable solid-state lasers, laser spectroscopy, and quantum electronics. In 2004 the Institute of Electrical Engineers in the United Kingdom has named Dr. Mirov and his team recipients of the Snell Premium award for the input in optoelectronics and development of Cr^{2+}:ZnS mid-IR external cavity and microchip lasers. Dr. Mirov is a member of the Optical Society of America, the American Physics Society, International Society for Optical Engineering, and Direct Energy Professional Society. He has authored or co-authored over three hundred scientific publications in the field of quantum electronics, has published 1 book, several book chapters, and holds fifteen patents.

Vladimir V. Fedorov was born in Moscow, Russia in 1961. He received the M. S. degree in physical and quantum electronics from the Moscow Institute of Physics and Technology, in 1985 and the Ph. D. degree in physics from the General Physics Institute of the Russian Academy of Sciences, Moscow, for his work on color center lasers and laser spectroscopy of the Rare Earth aggregate centers in the fluoride crystals. He joined General Physics Institute of the Russian Academy of Sciences, as a research fellow in 1987. His research interest include coherent and laser spectroscopy of doped solids; nonlinear optics; color center physics; and solid state lasers. Since 2000, he has a been working as a research associate and research assistant professor at the Department of Physics of the University of Alabama at Birmingham (UAB), USA. During the last years his research was concentrated on studying of laser media based on semiconductor materials with transition metal impurities. Dr. Fedorov is a member of the Optical Society of America, and the International Society for Optical Engineering. Dr. Fedorov with colleagues received "Snell Premium" of the Institute of Electrical Engineers of the United Kingdom in 2004.

Igor S. Moskalev was born in Belarus, USSR in 1973. He received his bachelor degree in physics from Novosibirsk State University, Russia in 1996 and till 1998 he worked as a research assistant in the Institute of Laser Physics, Novosibirsk, Russia, where he was involved in development of a highly stable, single frequency, diode pumped Nd:YAG laser with intracavity frequency doubling. Since 1998 till 1999 he worked as a research assistant in Hong Kong University of Science and Technology where he studied algal motility using a modified laser PIV system. He joined the Department

© 2010 by WILEY-VCH Verlag GmbH & Co. KGaA, Weinheim

of Physics of the University of Alabama at Birmingham (UAB), USA in 2000 and received his M. S. degree in physics in 2002, and his Ph. D. degree in physics in 2004 from UAB for his work on development of ultrabroadband, multiwavelength, tunable semiconductor and Cr^{2+}:ZnSe solid-state lasers. Currently he is involved in development of novel laser systems based on semiconductor materials with transition metal impurities. Dr. Moskalev is a member of the Optical Society of America. With colleagues, he received the "Snell Premium" of the Institute of Electrical Engineers of the United Kingdom in 2004 for development of Cr^{2+}:ZnS mid-IR external cavity and microchip lasers.

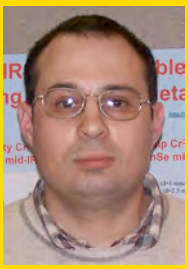

Dmitri V. Martyshkin was born in Russia in 1973. He received his bachelor degree from Novosibirsk State University, Russia in 1996. He received his master degree and his Ph. D. in Physics from University of Alabama at Birmingham, USA in 2000 and 2004 respectively. Dr. Martyshkin is involved in application of laser spectroscopy such as Raman, fluorescence, surface enhanced Raman spectroscopy (SERS), laser induced breakdown spectroscopy (LIBS), and cavity ring-down spectroscopy (CRDS) for biomedical applications. He is also involved in development and characterization of novel materials for laser and biomedical applications.

Changsu Kim was born in South Korea in 1973. He received his bachelor and master degree in media and telecommunication engineering from Ibaraki University, Japan in 2002 and 2004, respectively. In 2005, He joined the Department of physics of the University of Alabama at Birmingham (UAB), Alabama, USA, where he started pursuing the Ph. D. degree. His research interests include optical, laser spectroscopic, and electrical characterization of transition metal doped ZnSe, ZnS and CdSe nano- and microcrystals.

References

[1] A. A. Kaminskii, Laser & Photon. Rev. **1**, 93 (2007).
[2] A. A. Kaminskii, Crystalline Lasers: Physical Properties and Operating Schemes (CRC Press, Boca Raton, FL 1996).
[3] L. D. DeLoach, R. H. Page, G. D. Wilke, S. A. Payne, and W. F. Krupke, IEEE J. Quantum Electron. (USA) **32**, 885 (1996).
[4] T. Sorokina, Opt. Mater. **26**, 395 (2004).
[5] S. Mirov, V. Fedorov, I. Moskalev, and D. Martyshkin, IEEE J. Sel. Top. Quantum Electron. (USA) **13**(3), 810 (2007).
[6] B. Henderson and R. H. Bartram, Crystal-field Engineering of Solid-state Laser Materials (Cambridge University Press, Cambridge, 2000).
[7] O. Rössler and M. Schulz, New Series Vol. 41B: II–VI and I–VII Compounds; Semimagnetic Compounds (Springer Verlag, Berlin, 1999).
[8] J.-O. Ndap, C. I. Rablau, K. Morrow, O. O. Adetunji, V. A. Johnson, K. Chattopadhyay, R. H. Page, and A. Burger, J. Electron. Mater. **31**, 805 (2002).
[9] A. Burger, K. Chattopadhyay, J.-O. Ndap, X. Ma, S. H. Morgan, C. I. Rablau, C.-H. Su, S. Feth, R. H. Paged, K. I. Schaffersd, and S. A. Payne, J. Cryst. Growth **225**, 249 (2001).
[10] A. Sennaroglu, U. Demirbas, A. Kurt, and M. Somer, IEEE J. Sel. Top. Quantum Electron. (USA) **13**, 823 (2007).
[11] V. V. Fedorov, S. B. Mirov, A. Gallian, D. V. Badikov, M. P. Frolov, Yu. V. Korostelin, V. I. Kozlovsky, A. I. Landman, Yu. P. Podmar'kov, V. A. Akimov, and A. A. Voronov, IEEE J. Quantum Electron. (USA) **42**, 907 (2006).
[12] W. Mallory, V. V. Fedorov, S. B. Mirov, U. Hömmerich, W. Palosz, and S. B. Trivedi, J. Cryst. Growth **310**, 4438 (2008).
[13] J. J. Adams, C. Bibeau, R. H. Page, D. M. Krol, L. H. Furu, and S. A. Payne, Opt. Lett. **24**, 1720 (1999).
[14] J. Kernal, V. V. Fedorov, A. Gallian, S. B. Mirov, and V. V. Badikov, Opt. Express **13**, 10608 (2005).
[15] S. O. Kasap and P. Capper, Springer Handbook of Electronic and Photonic Materials (Springer, New York, 2006).
[16] K. Byrappa and T. Ohachi, Crystal Growth Technology (Springer, Berlin, 2003).
[17] V. A. Akimov, M. P. Frolov, Yu. V. Korostelin, V. I. Kozlovsky, A. I. Landman, Yu. P. Podmar'kov, and A. A. Voronov, phys. stat. sol. (c) **3**, 1213 (2006).
[18] C. H. Su, S. Feth, M. P. Volz, R. Matyi, M. A. George, K. Chattopadhyay, A. Burger, and S. L. Lehoczky, J. Cryst. Growth **207**, 35 (1999).
[19] V. Kasiyan, Z. Dashevsky, R. Shneck, and E. Towe, J. Cryst. Growth **290**, 50 (2006).
[20] J.-O. Ndap, O. O. Adetunji, K. Chattopadhyay, C. I. Rablau, S. U. Egarievwe, X. Ma, S. Morgan, and A. Burger, J. Cryst. Growth **211**, 290 (2000).
[21] U. N. Roy, O. S. Babalola, J. Jones, Y. Cui, T. Mounts, A. Zavalin, S. Morgan, and A. Burger, J. Electron. Mater. **34**, 19 (2005).
[22] S. B. Trivedi, C. C. Wang, S. Kutcher, U. Hommerich, W. Palosza, J. Cryst. Growth **310**, 1099 (2008).
[23] K. Grasza, S. B. Trivedi, Z. Yu, S. W. Kutcher, and G. A. Brost, J. Cryst. Growth **174**, 263 (1997).
[24] M. K. Udo, M. Villeret, I. Miotkowski, A. J. Mayur, A. K. Ramdas, and S. Rodriguez, Phys. Rev. B, Condens. Matter **46**, 7459 (1996).
[25] R. Pappalardo and R. D. Dietz, Phys. Rev. (USA) **123**, 1188 (1961).
[26] J.-O. Ndap, K. Chattopadhyay, O. O. Adetunji, D. E. Zelmon, and A. Burger, J. Cryst. Growth **240**, 176 (2002).
[27] U. Demirbas, A. Sennaroglu, and M. Somer, Opt. Mater. **28**, 231 (2006).
[28] E. Carnall, S. E. Hatch, and W. F. Parsons, Mater. Sci. Res. Int. **3**, 165 (1966).

© 2010 by WILEY-VCH Verlag GmbH & Co. KGaA, Weinheim

[29] J. Lu, K. Takaichi, T. Uematsu, J. F. Bisson, Y. Feng, A. Shirakawa, K. Ueda, H. Yagi, T. Yanagitani, and A. A. Kaminskii, Appl. Phys. B., Lasers Opt. **79**, 25 (2004).
[30] A. Gallian, V. V. Fedorov, S. B. Mirov, V. V. Badikov, S. N. Galkin, E. F. Voronkin, and A. I. Lalayants, Opt. Express **14**, 11694 (2006).
[31] C. Kim, D. V. Martyshkin, V. V. Fedorov, and S. B. Mirov, Opt. Express **16**, 4952 (2008).
[32] C. Kim, D. V. Martyshkin, V. V. Fedorov, and S. B. Mirov, Opt. Commun. submitted (2008).
[33] M. A. Noginov and V. S. Letokhov, Solid-State Random Lasers (Springer, New York, 2005).
[34] A. Gallian, V. V. Fedorov, J. Kernal, J. Allman, S. B. Mirov, E. M. Dianov, A. O. Zabezhaylov, and I. P. Kazakov, Appl. Phys. Lett. **86**, 091105 (2005).
[35] B. L. VanMil, A. J. Ptak, L. Bai, L. J. Wang, M. Chirila, N. C. Giles, T. H. Myers, and L. Wang, J. Electron. Mater. **31**, 770 (2002).
[36] Y. G. Sadofyev, V. F. Pevtsov, E. M. Dianov, P. A. Trubenko, and M. V. Korshkov, J. Vac. Sci. Technol. B, Microelectron. Nanometer Struct. **19**, 1483 (2001).
[37] M. Luo, B. L. Vanmil, R. P. Tompkins, Y. Cui, T. Mounts, U. N. Roy, A. Burger, T. H. Myers, and N. C. Giles, J. Electron. Mater. **32**, 737 (2003).
[38] J. E. Williams, R. P. Camata, V. V. Fedorov, and S. B. Mirov, Appl. Phys. A, Mater. Sci. Process. **91**, 333 (2008).
[39] S. Wang, S. B. Mirov, V. V. Fedorov, and R. P. Camata, Proceedings of Solid State Lasers XIII: Technology and Devices 5332 (SPIE, Bellingham, WA, 2004). pp. 13–19.
[40] M. S. Vitiello, F. Rizzi, G. Scamarcio, A. Colli, and F. Martelli, AIP Conf. Proc. **709**, 446 (2004).
[41] C. Kim, D. V. Martyshkin, V. V. Fedorov, I. S. Moskalev, and S. B. Mirov, Spectroscopy **22**, 30 (2007).
[42] V. V. Fedorov, A. Gallian, I. Moskalev, and S. B. Mirov, J. Lumin. **125**, 184 (2007).
[43] R. H. Page, J. A. Skidmore, K. I. Schaffers, R. J. Beach, S. A. Payne, and W. F. Krupke, in: OSA Trends in Optics and Photonics, edited by C. R. Pollock and W. R. Bosenberg (Optical Society of America, Washington DC, 1997), pp. 208–210.
[44] E. Sorokin, I. T. Sorokina, and R. H. Page, in: OSA Trends in Optics and Photonics, Advances in Solid State Lasers Vol. 46, edited by S. Payne and C. Marshall (Optical Society of America, Washington DC, 2001), pp. 101–105.
[45] M. Mond, E. Heumann, G. Huber, H. Kretschmann, S. Kuck, A. V. Podlipensky, V. G. Shcherbitsky, N. V. Kuleshov, V. I. Levchenko, and V. N. Yakimovich, in: OSA Trends in Optics and Photonics, Advances in Solid State Lasers Vol. 46, edited by S. Payne and C. Marshall (Optical Society of America, Washington DC, 2001), pp. 162–165.
[46] G. J. Wagner, T. J. Carrig, R. H. Page, K. I. Schaffers, J. Ndap, X. Ma, and A. Burger, Opt. Lett. **24**, 19 (1999).
[47] T. J. Carrig, G. J. Wagner, W. J. Alford, and A. Zakel, in: Proceedings of SPIE Vol. 5460, Solid State lasers and Amplifiers, edited by A. Sennaroglu, J. Fujimoto, and A. R. Pollock, (SPIE, Bellingham WA, 2004) pp. 74–82.
[48] I. T.Sorokina, in: Springer Topics in Applied Physics Vol. 89, Crystalline Lasers, Solid State Mid-Infrared Laser Sources, edited by I. T. Sorokina and K. L. Vodopyanov, (Springer, Berlin, Heidelberg, 2004), pp. 255–349.
[49] U. Demirbas and A. Sennaroglu, Opt. Lett. **31**, 2293 (2006).
[50] T. J. Carrig, G. J. Wagner, A. Sennaroglu, J. Y. Jeong, and C. R. Pollock, Opt. Lett. **25**, 168 (2000).
[51] I. T. Sorokina, E. Sorokin, A. Dileeto, M. Tonelli, R. H. Page, and K. I. Schaffers, in: OSA Trends in Optics and Photonics, Advances in Solid State Lasers Vol. 50, edited by C. Marshall, (Optical Society of America, Washington DC, 2001), pp. 157–161.
[52] C. R. Pollock, N. A. Brilliant, D. Gwin, T. J. Carrig, W. J. Alford, J. B. Heroux, W. I. Wang, I. Vurgaftman, and J. R. Meyer, Advanced Solid State Photonics Vol. 98 (OSA, Washington DC, 2005).
[53] I. Sorokina and E. Sorokin, in: Advanced Solid-State Photonics 2007, WA7, Chirped-mirror Dispersion Controlled Femtosecond Cr:ZnSe Laser, Technical Digest on CD-ROM (The Optical Society of America, Washington DC, 2007).
[54] S. B. Mirov, V. V. Fedorov, K. Graham, I. S. Moskalev, V. V. Badikov, and V. Panutin, Advanced Solid State Lasers, edited by M. E. Fermann and L. R. Marshall (Optical Society of America, Washington DC, 2002), pp. 364–370.
[55] S. B. Mirov, V. V. Fedorov, K. Graham, I. Moskalev, V. Badikov, and V. Panyutin, Opt. Lett. **27**, 909 (2002).
[56] S. B. Mirov, V. V. Fedorov, K. Graham, I. S. Moskalev, V. V. Badikov, and V. Panutin, in: OSA Trends in Optics and Photonics (TOPS) Vol. 73, Conference on Lasers and Electro-Optics, OSA Technical Digest, Postconference Edition (Optical Society of America, Washington DC, 2002), pp. 120–121.
[57] S. B. Mirov, V. V. Fedorov, K. Graham, I. S. Moskalev, I. T. Sorokina, E. Sorokin, V. Gapontsev, D. Gapontsev, V. V. Badikov, and V. Panyutin, IEE Proc. J. Optoelectron. **150**(4), 340 (2003).
[58] B. McKay, W. B. Roh, and K. L. Schepler, in: OSA Trends in Optics and Photonics Vol. 73, Paper CMY3, Conference on Lasers and Electro-Optics, OSA Technical Digest, Postconference Edition (OSA, Washington DC, 2002), pp. 119–120.
[59] G. J. Wagner, B. G. Tiemann, W. J. Alford, and T. J. Carrig, in: Advanced Solid-State Photonics on CD-ROM, WB12 (The Optical Society of America, Washington DC, 2004).
[60] I. S. Moskalev, S. B. Mirov, and V. V. Fedorov, Opt. Express **12**, 4986 (2004).
[61] A. Gallian, V. V. Fedorov, J. Kernal, S. B. Mirov, and V. V. Badikov, Advanced Solid State Photonics on CD-ROM, MB12 (Optical Society of America, Washington DC, 2005).
[62] E. Sorokin and I. Sorokina, Appl. Phys. Lett. **80**, 3289 (2002).
[63] A. Gallian, V. V. Fedorov, S. B. Mirov, V. V. Badikov S. N. Galkin, E. F. Voronkin, and A. I. Lalayants, Technical Digest, CLEO'05, Baltimore, MD, May 22–27, 2005 (Optical Society of America, Washington DC, 2005).
[64] I. S. Moskalev, V. V. Fedorov, and S. B. Mirov, Opt. Express **16**, 4145 (2008).

© 2010 by WILEY-VCH Verlag GmbH & Co. KGaA, Weinheim

[65] G. J. Wagner and T. J. Carrig, in: OSA Trends in Optics and Photonics, Advances in Solid State Lasers Vol. 50, edited by C. Marshall (Optical Society of America, Washington DC, 2001), pp. 506–510.
[66] I. S. Moskalev, V. V. Fedorov, S. B. Mirov, P. A. Berry, and K. L. Schepler, ASSP Technical Digest on CD, WB30 (Opt. Soc. of Am., Washington DC, 2009).
[67] I. T. Sorokina, E. Sorokin, S. B. Mirov, V. V. Fedorov, V. Badikov, V. Panyutin, and K. Schaffers, Opt. Lett. **27**, 1040 (2002).
[68] K. Graham, S. B. Mirov, V. V. Fedorov, M. E. Zvanut, A. Avanesov, V. Badikov, B. Ignat'ev, V. Panutin, and G. Shevirdyaeva, in: OSA Trends in Optics and Photonics, Advanced Solid-State Lasers Vol. 50 (TOPS), edited by C. Marshall (Optical Society of America, Washington DC, 2001), p. 561–567.
[69] I. T. Sorokina, E. Sorokin, T. J. Carrig, and K. I. Schaffers, in: Advanced Solid State Photonics on CD-ROM, TuA4, (The Optical Society of America, Washington DC, 2006).
[70] I. S. Moskalev, V. V. Fedorov, and S. B. Mirov, Proc. SPIE – Int. Soc. Opt. Eng. **7193**, 7193–59 (2009).
[71] J. McKay, W. B. Roh, and K. L. Schepler, in: OSA Trends in Optics and Photonics, Advances in Solid State Lasers Vol. 68 (Optical Society of America, Washington DC, 2001), p. 371.
[72] J. McKay, W. B. Roh, and K. L. Schepler, in: OSA Trends in Optics and Photonics, Advances in Solid-State Lasers Vol. 68 (Optical Society of America, Washington DC, 2002), pp. 371–373.
[73] V. A. Akimov, V. I. Kozlovsky, Yu. V. Korostelin, A. I. Landman, Yu. P. Podmar'kov, Ya. K. Skasyrsky, and M. P. Frolov, Russ. Quantum Electron. **37**, 991 (2007).
[74] V. A. Akimov, V. I. Kozlovsky, Yu. V. Korostelin, A. I. Landman, Yu. P. Podmar'kov, Ya. K. Skasyrsky, and M. P. Frolov, Russ. Quantum Electron. **38**, 205 (2008).
[75] J. T. Seo, U. Hommerich, S. B. Trivedi, R. J. Chen, and S. Kutcher, Opt. Commun. **153**, 267 (1998).
[76] U. Hommerich, J. T. Seo, A. Bluiett, M. Turner, D. Temple, S. B. Trivedi, H. Zong, S. W. Kutcher, C. C. Wang, R. J. Chen, and B. Schumm, J. Lumin. **87**, 1143 (2000).
[77] A. G. Bluiett, U. Hömmerich, R. T. Shah, S. B. Trivedi, S. W. Kutcher, and C. C. Wang, J. Electron. Mater. **31**, 806 (2002).
[78] Yu. P. Podmar'kov, V. A. Akimov, M. P. Frolov, Yu. V. Korostelin, V. I. Kozlovsky, A. I. Landman, and Ya. K. Skasyrsky, International Conference on Laser Optics 2008, Technical Program, St. Petersburg, Russia, 2008 (Institute for Laser Physics, St. Petersburg, Russia, 2008), p. 59.
[79] E. Sorokin, S. Naumov, and I. T. Sorokina, Ultrabroadband infrared solid-state laser IEEE J. Sel. Top. Quantum Electron. (USA) **11**, 690 (2005).
[80] R. V. Ambartsumyan, N. G. Basov, P. G. Kryukov, and V. S. Letokhov, Pis'ma Zh. Eksp. Teor. Fiz. **3**, 261 (1966) (Russian), JETP Lett. (Russia) **3**, 167 (1966).
[81] R. Kaiser, C. Westbrook, and F. David, Coherent Atomic Matter Waves (Springer, Berlin, Heidelberg, 2001).
[82] D. S. Wiersma, P. Bartolini, A. Lagendijk, and R. Righini, Nature **390**, 671 (1997).
[83] D. V. Martyshkin, C. Kim, I. S. Moskalev, V. V. Fedorov, and S. B. Mirov, in: Conference on Lasers and Electro-Optics/Quantum Electronics and Laser Science Conference and Photonic Applications Systems Technologies 2008, Technical Digest, QED2 (Optical Society of America, Washington DC, 2008).
[84] D. V. Martyshkin, V. V. Fedorov, C. Kim, I. S. Moskalev, and S. B. Mirov, Phys. Rev. Lett. submitted (2008).
[85] A. A. Voronov, V. I. Kozlovskii, Yu. V. Korostelin, A. I. Landman, Yu. P. Podmar'kov, and M. P. Frolov, Russ. Quantum Electron. **35**, 809 (2005).
[86] V. A. Akimov, A. A. Voronov, V. I. Kozlovsky, Yu. V. Korostelin, A. I. Landman, Yu. P. Podmar'kov, and M. P. Frolov, Russ. Quantum Electron. **36**, 299 (2006).
[87] M. P. Frolov, Yu. V. Korostelin, V. I. Kozlovsky, A. I. Landman, Yu. P. Podmar'kov, Ya. V. Skasyrsky, and A. A. Voronov, International Conference on Laser Optics 2008, Technical Program, St. Petersburg, Russia, 2008 (Institute for Laser Physics, St. Petersburg, Russia, 2008), p. 60.
[88] S. B. Mirov, V. V. Fedorov, K. Graham, I. S. Moskalev, I. T. Sorokina, E. Sorokin, V. Gapontsev, D. Gapontsev, V. V. Badikov, and V. Panyutin, in: 5th International Conference on Mid-Infrared Optoelectronic Materials and Devices, September 8–11, Abstract Book (IEE Proceedings, Annapolis, MA, 2002), pp. 143–144.
[89] L. Luke, V. V. Fedorov, I. Moskalev, A. Gallian, and S. B. Mirov, in: Proceedings of SPIE Vol. 6100, Solid State Lasers XV: Technology and Devices, edited by H. J. Hoffman and R. K. Shori, 61000Y-1-8, ISBN 0-8194-6142-3, (SPIE, Bellingham, WE, 2006).
[90] S. B. Mirov and V. V. Fedorov, in: Mid-Infrared Coherent Sources and Applications, New Regimes of Excitation and Mid-IR Lasing of Transition Metal Doped II–VI Crystals, invited chapter, edited by M. Ebrahimzadeh and I. T. Sorokina, (Springer, Dordrecht, 2008), pp. 261–314.
[91] N. Balkan, Hot Electrons in Semiconductors: Physics and Devices (Oxford University Press, 1998).
[92] K. Katayama, H. Matsubara, F. Nakanishi, T. Nakamura, H. Doi, A. Saegusa, T. Mitsui, T. Matsuoka, M. Irikura, T. Takebe, S. Nishine, and T. Shirakawa, J. Cryst. Growth **214–215**, 1064 (2000).
[93] N. A. Vlasenko and Z. Popkov, Opt. Spectrosc. (Russia) **8**, 39 (1960).
[94] M. Godlewski and M. Kaminska, J. Phys. C, Solid State Phys. **13**, 6537 (1980).
[95] D. R. Vij, Handbook of the Electroluminescence Material (IOP Publishing London, UK, 2004).
[96] E. Bringuie, J. Appl Phys. (USA) **70**(8) 4505, (1991).
[97] F. Capasso, in: Semiconductors and Semimetals Vol. 22, edited by R. K. Willardson and A. C. Beer (Academic Press, New York, 1985), Part D, p. 1.
[98] C. Kim, J. Peppers, D. V. Martyshkin, V. V. Fedorov, and S. B. Mirov, Proc. SPIE – Int. Soc. Opt. Eng. **7193**, 7193–110 (2009).
[99] N. A. Vlasenko, P. F. Oleksenko, Z. L. Denisova, M. A. Mukhlyo, and L. I. Veligura, Semicond. Phys. Quantum Electron. Optoelectron. **10**, 87 (2007).
[100] J. Jaeck, R. Haidar, E. Rosencher, M. Caes, M. Tauvy, S. Collin, N. Bardou, J. L. Pelouard, F. Pardo, and P. Lemasson, Opt. Lett. **31**, 3501 (2006).
[101] N. A. Vlasenko, Z. L. Denisova, Ya. F. Kononets, L. I. Veligura, and Yu. A. Tsyrunov, J. Soc. Inf. Disp. **12**, 179 (2004).

© 2010 by WILEY-VCH Verlag GmbH & Co. KGaA, Weinheim

[102] N. A. Vlasenko, P. F. Oleksenko, Z. L. Denisova, M. O. Mukhlyo, and L. I. Veligura, phys. stat. sol. (b) **245**, 2550 (2008).
[103] M. Godlewski, A. J. Zakrzewski, and V. Yu. Ivanov, J. Alloys Compd. **300–301**, 23 (2000).
[104] M. Surma and M. Godlewski, Radiat. Eff. Defects Solids (UK) **135**, 213 (1995).
[105] B. M. Kimpel, K. Lobe, H. J. Schulz, and E. Zeitler, Meas. Sci. Technol. **6**(9), 1383 (1995).
[106] R. N. Bhargava, D. Gallagher, X. Hong, and A. Nurmikko, Phys. Rev. Lett. **72**(3), 416 (1994).
[107] P. H. Borse, N. Deshmukh, R. F. Shinde, S. K. Date, and S. K. Kulkarni, J. Mater. Sci. (Netherlands) **34,** 6087 (1999).
[108] P. Yang, M. Lü, D. Xü, D. Yuan, J. Chang, G. Zhou, and M. Pan, Appl. Phys. A **74**, 257 (2002).
[109] P. Koranda, H. Jelínkova, J. Sulc, M. Nemec, M. E. Doroshenko, T. T. Basiev, V. K. Komar, and M. B. Kosmyna, Opt. Mater **30**, 149 (2007).

© 2010 by WILEY-VCH Verlag GmbH & Co. KGaA, Weinheim